C.P. No. 884

C.P. No. 884

MINISTRY OF AVIATION

AERONAUTICAL RESEARCH COUNCIL

CURRENT PAPERS

An Experimental Investigation of the Flow Through Inclined Circular Tubes at a Mach Number of 4.0

by

P. L. Roe

LONDON: HER MAJESTY'S STATIONERY OFFICE

1966

PRICE 8s 6d NET

U.D.C. No. 532.542.1 : 533.697.2 : 533.6.011.5

C.P. No. 884
May 1965

AN EXPERIMENTAL INVESTIGATION OF THE FLOW THROUGH INCLINED CIRCULAR TUBES AT A MACH NUMBER OF 4.0

by

P. L. Roe

SUMMARY

Pressure plotting experiments have been performed on the internal flow through inclined circular tubes at M = 4, and the results used to investigate both the nature of the flow and the internal forces. It is intended to apply the results to the wind tunnel testing of models with nacelles. Linear theory calculations have been made and the predicted forces are in good agreement with experimental values, provided the ducts are short.

Replaces R.A.E. Technical Report 65110 - A.R.C. 27183

CONTENTS

1 INTRODUCTION

An aircraft or missile designed to fly at moderate to high Mach numbers propelled by air breathing engines will normally have engine intakes whose capture area is a considerably large fraction of the total cross-section of the vehicle. A wind tunnel model intended to give a realistic representation of external flow must therefore swallow the correct volume of air. If the power plant itself is not to be represented the easiest solution is to allow the captured air to flow through simple tubes and exhaust back into the main stream. Such an arrangement has been frequently used and, if the tube is not too long and the Mach number not too low, supersonic flow will be established throughout the tube, the shock pattern will be attached, and the inlet will run full[1]. It usually seems to have been assumed that under these conditions the internal flow contributes significantly to the drag forces on the model, but not to any transverse forces, except in a short region just behind the inlet. This region gives rise to inlet forces similar to those experienced on the real aircraft. Behind this region the highly dissipative influence of shocks, boundary layers, and their mutual interactions are assumed to lead to the rapid annihilation of any transverse momentum.

At high supersonic Mach numbers, however, when the shock system within the tube is strong and relatively little inclined to the axis, we might expect a strongly patterned flow to persist for some distance downstream, and the possibility of the internal flow making a sizeable contribution to the transverse forces cannot be excluded without testing.

Since such effects would evidently not correspond to any situation obtaining in the case of the real aircraft plus power plant, it will be desirable to measure or estimate them somehow, so that they may be subtracted out from the forces observed in wind tunnel testing.

These considerations became apparent during the planning of a series of tests involving the addition of cylindrical nacelles to a series of basic missile models. When it appeared that no reliable method for estimating the transverse forces existed, a series of subsidiary tests was put in hand, to provide internal pressure plots on isolated nacelles. As it was felt that these results would have some general interest they are presented here separately from those of the main tests.

2 DESCRIPTION OF MODELS AND APPARATUS

The three models which were tested are illustrated in Figs.1 and 2. Two of these, B and C, were simply geometrical reproductions of nacelles used in

the missile tests mentioned in the introduction. These were steel tubes with an internal diameter of 3.450 in and an external diameter of 3.700 in. The overall lengths of the two nacelles were 23.670 in and 15.900 in and a 10° chamfer was cut internally on the intake. Since the boundary layer would presumably be thickened by interaction with the shock pattern inside the tube it seemed quite possible that it might allow disturbances from the exit to be propagated upstream, and the intention of the shorter tube was to check this point by comparison with the front portion of the longer tube.

Additionally it was felt that more general interest would be obtained from a tube whose interior was a simple parallel bore, and so a third model was constructed with the intake chamfered externally. This is known as tube A, and will receive the most attention in this Report.

Each model had a row of half-millimetre diameter static pressure holes spaced at $\frac{3}{4}$ in intervals along a generator of the tube with an additional hole $\frac{3}{8}$ in from the intake. The tubes were mounted on short pylons which could be fitted onto a sting and quadrant support (Figs.1 and 2). After setting the quadrant to the desired incidence the model could then be rolled around the sting to bring the row of pressure holes into any circumferential position relative to the wind direction. Pressures were measured on a set of self balancing weighbeam manometers.

All tests were made in the High Supersonic Speed Tunnel at R.A.E. Bedford at a free stream Mach number of 3.97. The Reynolds number of the detailed investigations was 2.24×10^{6} based on internal diameter, but a brief look was taken at the qualitative effects of varying Reynolds number within the range $1.12 - 2.74 \times 10^{6}$. The total temperature was held constant at 40°C and the humidity was maintained below 200 ppm.

3 MEASUREMENTS PERFORMED

Owing to the symmetry of a circular cylinder, it is not necessary to make any distinction between incidence and yaw. Thus the attitude is defined solely by the incidence, α, and all the models were tested at $\alpha = 5$, 10, 15 and 20°, in each case with the row of pressure holes being moved round by 15° steps from $\psi = 0$ (bottom dead centre) to $\psi = 180^{\circ}$.

The pressures so obtained were integrated to yield normal force and pitching moment coefficients using the DEUCE computer at R.A.E. Bedford working on a programme based on Simpson's rule. Linear extrapolation was used to find the pressures at the tip. On the assumption that any trailing edge effect propagated upstream through the boundary layer was so small that the pressures

back to a particular station were substantially the same as if the tube had ended at that station, the integration of pressures between limits $x = 0$ and $x = \ell$ was taken to give the forces on a tube of length ℓ. It appears from the comparison between models B and C (Section 4.5) that this assumption was valid except for the highest incidence.

To reduce the time taken in making measurements it was further assumed that the flow in the tube possessed symmetry about the incidence plane. Check points taken during the tests suggested that this was in fact so, and that even if the fine detail of the pressure distribution was not repeatable from one side to the other, the effect of such asymmetry on the overall forces was very small.

Some hysteresis effects were observed with model A at incidences close to 10°. These are noted briefly here, but the time was not available to investigate them in detail.

4 DISCUSSION OF RESULTS

4.1 Preliminary

For the simple case of two-dimensional flow in a parallel sided rectangular duct; supersonic linear theory predicts the flow pattern shown in Fig.3, taken from Ref.2. The shock and the expansion wave generated at the lip are reflected down the tube without any change in strength, and the pressure distributions along the upper and lower inside surfaces are two square waves of period $2\ell/\beta h$ in antiphase. The lift acting locally on a particular part of the tube may be positive or negative, and if the length is an exact multiple of $2\ell/\beta h$ the tube will experience no resultant lift but only a pitching moment.

In practice[2,3], it is found that the predicted periodic disturbances are attenuated with increasing distance down the duct, so that C_p, C_N, etc, have the character of damped oscillations.

For very long ducts we may assume that the flow eventually becomes parallel at a sufficiently large distance downstream. Under these conditions C_p will be a function of x only, and C_N, from consideration of momentum changes normal to the tube axis, will tend to the constant value $2 \sin \alpha \cos \alpha$ independently of cross section shape.

The cylindrical duct is a more complicated theoretical problem, and in fact no solution has been found for ducts with finite length greater than $2\beta r$, but physically one would expect the same type of solution. That is, a damped periodic flow in which $C_p \rightarrow C_p(x)$ and $C_N \rightarrow 2 \sin \alpha \cos \alpha$.

4.2 Pressure distributions

The pressure distributions along the top and bottom generators of models 'A' and 'B' at zero incidence are shown in Fig.4. The internal chamfer on model 'B' gives rise to pressure peaks which reflect down the tube. It is seen that similar pressure peaks are present, on a reduced scale, in model 'A'. These are presumably due to the internal boundary layer displacement thickness giving model 'A' an effective shape which is, at least at zero incidence, similar to that produced by chamfering.

With the particular model support system used (Figs.1 and 2) measurements on different tube generators were made with the model in different parts of the tunnel airstream. As the flow direction in the tunnel is known[5] to vary from point to point by angles of the order of $\pm\frac{1}{4}^{\circ}$, this is a source of error. Comparison of the results for top and bottom generators shown in Fig.4 indicates that these errors are fairly small and certainly negligible for present purposes.

Contour maps of static pressures are presented in Figs.5 and 6. Regions of negative C_p are shown cross hatched, and the contours are labelled with the value of $\beta C_p/2\alpha$, which is the ratio of pressure coefficient as measured to the two-dimensional linear theory value.

Fig.5 presents results for the internally parallel model A. The reflected pressure and suction peaks are clearly seen. It is interesting to note that at low incidence ($\alpha = 5^{\circ}$) the second and third pressure peaks (on the lower and upper generators respectively) are augmented above the value reached by the first peak, rather than attenuated below it. This is probably related to the fact that some "focussing"[4] of the curved leading edge shock must occur, which will cause it to become steeper and stronger. A further effect of this focussing can be observed by noting that the position where the shock reaches the bottom generator (marked by the steep pressure rise along $\psi = 0$) is well forward of its linear theory position at $x/\beta r = 2.0$.

At higher incidences the attenuation of pressure peaks begins at once, and at $\alpha = 15^{\circ}$ and $\alpha = 20^{\circ}$ the circumferential pressure differences are already small at the back end.

The results for model B, which has an internally chamfered leading edge, are presented in Fig.6. The main differences to be noted are the generally higher pressure peaks, and the fact that the shock system as a whole has contracted lengthwise. Both of these effects are presumably associated with

the decrease in Mach number brought about by the internal area contraction, and both may also be noted in the zero incidence comparisons of Fig.4.

4.3 Normal force

The normal force coefficient C_N is defined as:-

$$C_N(\ell) = \frac{1}{\pi R^2} \int_0^{\ell} dx \int_0^{2\pi} C_p \cos\psi \; (r\,d\psi) \; . \qquad (1)$$

This represents the normal force due to the internal flow, acting on that portion of the tube which was between $x = 0$ and $x = \ell$.

We also have from linear theory (Refs.6-8 and Appendix to present Report)

$$C_N(\ell) = 2\alpha V_1\left(-\frac{\ell}{\beta r}\right) \qquad (2)$$

where V_1 is a function which may be evaluated numerically for $-2 < \ell/\beta r < +\infty$. Within linear theory there is no lift due to thickness (as for example the chamfer on models B and C).

A comparison between the experimental forces (equation (1) and (2)) is made for model A in Fig.7 and for model B in Fig.8. It will be seen that for tube lengths less than about $1\beta r$ the agreement in the case of model A is quite extraordinarily good even at the highest incidence. This agreement may appear rather fortuitous, especially in view of the complicated detail pressure distributions revealed by Fig.5, and it cannot be maintained without further investigation that equally successful predictions could be made at all other Mach numbers or Reynolds numbers. However, it is known from many other applications, e.g. thin airfoil theory, that linear theory may often give good estimates of overall forces even when local pressures are considerably in error.

For lengths between $1\beta r$ and $2\beta r$ the experimental and theoretical curves begin to diverge, best agreement being naturally maintained for the lower incidences.

The linear theory solution has a singularity at $x = 2\beta r$ invalidating any solution for longer tubes, which must necessarily be investigated experimentally.

Fig.8 shows the analogous results for model B. Best agreement with theory is obtained if the reference area in C_N is taken to be the inlet area, while the reference length r in $x/\beta r$ is taken as the final parallel radius of the duct.

If this is done fairly close agreement is obtained between the experimental points and the theoretical curve for sufficiently short ducts.

In Fig.9 is shown internal normal force against incidence for parallel tubes of various lengths. For a short tube, $(\ell/\beta r = 0.45)$, such as is shown by Fig.7 to coincide with linear theory, the variation of force with incidence is linear. However, for longer tubes, we see that marked non-linear effects are present. In general, these appear at lower incidences as the tube length is increased. Fig.9 also includes the slender theory estimates $(C_n = 2 \sin\alpha \cos\alpha)$ which may be seen to give progressively better results as tube length increases.

4.4 Pitching moment

Pitching moment coefficient C_M is defined as:-

$$C_M(\ell) = \frac{1}{(\pi R^2)\, r} \int_0^{\ell} x\, dx \int_0^{2\pi} Cp \cos\psi \; (r\, d\psi) \qquad (3)$$

and experimental results based on the definition are compared with the linear theory result (see Appendix):-

$$C_M(\ell) = 2\alpha\beta\, M\left(-\frac{\ell}{\beta r}\right) \quad . \qquad (4)$$

In equation (3) the inlet area πR^2 is used as reference area, since this appears to be most closely associated with the forces experienced (Section 4.3), but the final radius r is chosen as reference length, as this is more closely related to the periodicity.

Since a correct prediction of the lift distribution along the tube automatically implies a correct prediction of the pitching moments, linear theory applies here to the same cases discussed in the previous sub-section.

Note that for a sufficiently long tube, $C_M(\ell)$ tends to some finite constant value, since if the part of the tube downstream of some station makes no contribution to the lift, it makes no contribution to the pitching moment either.

4.5 Comparison between models 'B' and 'C'

It has so far been assumed that conditions at exit from the tube have no effect on the flow within the tube: that is to say there is no significant

upstream influence through any region of subsonic flow, so that the pressures over the foremost portion of any tube are independent of the length of that tube. Models 'B' and 'C' were intended to check on this assumption. Geometrically they were reproductions of the removable nacelles used in the main tests (see Sections 1 and 2) and differed only in their overall lengths.

Full pressure plots were obtained for both models at incidences $0(5)20^\circ$, and only for $\alpha = 20^\circ$ were any significant differences observed. At this incidence, however, quite large systematic discrepancies between the two models were to be found.

These are brought out by Figs.13-15. Fig.13 shows the pressure distributions on the two models. The main difference is that the region of very high pressure found near the top of the tube just behind the inlet is of rather smaller extent on model C than on model B. The effect which this has on normal force and pitching moment coefficients is shown in Figs.14 and 15. At lower incidences the two curves are almost indistinguishable (see Fig.14(b)).

A possible interpretation of these results is that at higher incidences the stronger shock system produces thicker boundary layers and separation regions, which can more easily carry trailing edge influence upstream. In any case the results derived in this Report for $\alpha = 20^\circ$ cannot be regarded as better than 10% accurate. However, the results for lower incidences seem more solidly based.

4.6 A hysteresis phenomenon

At incidences near 10° it was found that two distinct pressure distributions could be obtained for the same model at the same incidence. The main determining factor appeared to be the direction from which the incidence was approached when setting up the model attitude, although there was some indication that even when the model was held at constant incidence, one pattern might change spontaneously into the other. Differences between the two patterns were most significant in the region of negative C_p just behind the inlet. The effect was strongly dependent on Reynolds number, and a detailed investigation would have involved lengthy testing which was not felt to be justified, especially as the difference in overall forces produced was fairly small (less than 5%). However, some results and a tentative explanation are put forward in this section.

Fig.16 shows six different pressure distributions obtained from model A at $\alpha = 10^\circ$. In each case the pressures are measured along the bottom generator ($\dot{y} = 0$) for $0 < x/\beta r < 1.5$. For each of three different Reynolds numbers the

test attitude was approached either from very low ($\alpha \simeq 0^{\circ}$) or from very high ($\alpha \simeq 20^{\circ}$) incidence. It will be observed that in each case the direction of approach makes a considerable difference. At lower incidences (α less than about 8°) the pressure distribution is independent of the direction from which the attitude is approached, and has the typical general shape of Fig.17. At high incidence the pattern is again unique at a given attitude but changes rapidly with incidence.

The behaviour is apparently linked with the tendency of the boundary layer on the lower surface to separate owing to interaction with the shock from the upper lip.

The point at which separation appears to occur is marked as 'S' on each of the diagrams in Figs.16, 17 and 18*. At low incidences when the shock is weak separation occurs well down the tube (Fig.17) while at high incidences the separation region extends forward right to the leading edge (Fig.18(c)). At intermediate incidences the hysteresis effect is present (Fig.16).

The position of the point S as a function of incidence for three different Reynolds numbers is plotted in Fig.19, which also shows the approximate location of the shock. The main features of these plots are reproduced schematically in Fig.20.

Suppose the model to be initially at some small incidence, and the boundary layer to be laminar right back to the shock, which induces laminar separation a short distance ahead of itself (point U of Fig.20). As the incidence is increased and the shock becomes stronger the separation point moves forward along UT until, near T, transition to turbulent flow occurs and S consequently moves back to T' (compare Figs.16(a)(iii) and 18(a)). With still further increase of incidence S moves forward again, following the new curve T'F, until at F it reaches the leading edge. If incidence is now reduced, S moves back again along FT', but the change back from turbulent to laminar flow does not take place at T'. Instead turbulence persists until the point R is reached. It should be noted that there is no direct evidence for the state of the boundary layer. In any future similar tests it would be desirable to try the effect of transition fixing.

A typical variation with incidence of the pressure at a fixed point is shown in Fig.21.

---

* S has actually been taken as the point at which the pressure rise due to separation begins; this is not strictly the same as the separation point, but its movement will be associated with the movement of the true separation point, and this suffices for present interests.

The results given in previous sections for models 'A' and 'B' at $\alpha = 10^{\circ}$ were for the turbulent boundary layer condition.

4.7 Comparison with other data

Cook[2,3] has presented the results of force measurements on circular ducts at Mach numbers between 1.4 and 2.2. His models had values of ℓ/r equal to 2.78, 5.56, and 8.34, and the Reynolds numbers of his tests lay between 2.0×10^5 and 3.0×10^5 on internal diameter. Although his results do not distinguish between the internal and external contributions a limited comparison may be made as follows.

At very small incidences the external forces will be represented accurately by linear theory, even though the internal forces (which are more strongly influenced by viscous effects) may not be so represented. Thus, if from Cook's measured $(\partial C_M/\partial\alpha)_{\alpha=0}^{TOTAL}$ the linear theory estimate of $(\partial C_N/\partial\alpha)_{\alpha=0}^{EXT}$ is subtracted, an approximation to the internal contribution to initial lift slope is obtained.

This has been done for the results of Fig.31 of Ref.3, on the assumption that the external forces on Cook's model are the same as for an externally parallel duct of the same final external diameter. The results are shown in Fig.22. It is seen that the estimates so obtained are in good agreement with the present tests for the lower values of $\ell/\beta r$. The poor agreement at higher values may be due to the difference in Reynolds number, or to a failure of the method for estimating the external contribution.

5 CONCLUSIONS

(1) The internal forces on circular ducts for which $\ell/\beta r < 1.0$ are well represented by linear theory.

(2) Slender theory is not adequate to predict the forces on any model in the present set of tests but it gives progressively better results as $\ell/\beta r$ increases.

(3) The presence of an internal contraction in the duct may affect the results considerably.

(4) Boundary layer effects are important; in particular they lead to an incidence hysteresis phenomenon.

ACKNOWLEDGEMENTS

Thanks are due to P.H. Cook and D.A. Treadgold of R.A.E. Farnborough for discussions and pre-publication access to the results of Ref.2, and to Miss Sandra Willmot, of R.A.E. Bedford Computing Section, who wrote the DEUCE programme for the pressure integration.

Appendix A

LINEAR THEORY OF SUPERSONIC FLOW THROUGH A PARALLEL CIRCULAR DUCT AT INCIDENCE

This problem is a special case of the theory of quasi-cylindrical ducts developed by Ward in Refs.6 and 7 and by Lighthill in Ref.8. We follow here the notation, etc, of Ref.7. It is shown there that the pressure coefficient at a point (x, r_o, θ) on the inner wall of the duct is given by

$$C_p = \frac{2\alpha \cos\theta}{\beta} V_1'\left(-\frac{x}{\beta r_o}\right) \qquad (A.1)$$

where $V_1'(z)$ is a function given by the equation (8.5.16 of Ref.7)

$$V_1'(z) = e^{-0.6453\,z}\{1.2120 \cos 0.5012\,z + 0.1898 \sin 0.5012\,z\} - \int_0^\infty \frac{e^{-\lambda z}}{K_1'^2(\lambda) + \pi^2 I_1'^2(\lambda)} \frac{d\lambda}{\lambda^2} \qquad (A.2)$$

where $I_1'(\lambda)$ and $K_1'(\lambda)$ are the first derivatives of the first order modified Bessel functions of the 1st and 2nd kinds.

The values assumed by this function for positive values of z are relevant to the theory of the external flow past ducts and are given in Refs.6 and 7. For $0 \geq z > -2$, equation (A.2) can be evaluated to yield, via equation (A.1), the internal pressures. For $z < -2$, the infinite integral in equation (A.2) does not converge, and no linear theory solution has yet been found.

The following properties of $V_1'(z)$ are given by Ward.

(a) For small z,

$$V_1'(z) = 1 - \frac{1}{2} z - \frac{1}{16} z^2 + \ldots. \qquad (A.3)$$

(in Ref.6 the coefficient of z^2 is given, erroneously, as $-\frac{11}{32}$).

(b) $V_1'(z)$ has a logarithmic singularity at $z = -2$, and as z approaches -2 from above, (Ref.6)

$$V_1'(z) \to -\frac{2}{\pi} \log \frac{1}{2+z} + O(1) \quad \ldots. \tag{A.4}$$

Two related functions, V_1 and M are defined by

$$V_1(z) = \int_o^z V_1'(z)\, dz \tag{A.5}$$

$$M(z) = \int_o^z V_1'(z)\, z\, dz \quad . \tag{A.6}$$

These enable the lift and pitching moment acting on a duct of length ℓ to be found as

$$C_L(\ell) = 2\alpha V_1\left(-\frac{\ell}{\beta r}\right) \tag{A.7}$$

$$C_M(\ell) = 2\alpha\beta\, M\left(-\frac{\ell}{\beta r}\right) \quad . \tag{A.8}$$

Equation (A.2) has been used to evaluate $V_1'(z)$ in the interval $0 > z > -1.95$. The integral in equation (A.2) was evaluated graphically within the range $0 < \lambda < 10$. For $z < -1.5$ the contribution from $\lambda > 10$ is significant and was calculated from the appropriate asymptotic expansions. V_1 and M were then found from (A.5) and (A.6). All three functions are presented in Table 1.

Table 1

THE FUNCTIONS V_1', V_1 AND M

z	$V_1'(-z)$	$V_1(-z)$	$M(-z)$
0	1.000	0	0
0.2	1.090	0.209	0.021
0.4	1.175	0.436	0.089
0.6	1.255	0.679	0.211
0.8	1.305	0.935	0.391
1.0	1.300	1.197	0.626
1.2	1.210	1.449	0.904
1.4	1.030	1.670	1.196
1.6	0.725	1.853	1.463
1.8	0.100	1.942	1.611
1.9	-0.540	1.923	1.577
1.95	-1.094	1.882	1.498
2.0	$-\infty$		

NOTATION

(x,r,ψ)	cylindrical coordinates
h	half-height of rectangular duct
ℓ	length of duct
q_∞	free stream dynamic pressure
r	internal radius of parallel portion of duct
z	$= x/\beta r$
C_p	pressure coefficient
C_L	lift coefficient } based on inlet area
C_N	normal force coefficient } based on inlet area
C_M	pitching moment coefficient, based on inlet area and r, origin at centre of inlet
M	Mach number, function defined in Appendix A
R	inlet radius
Re	Reynolds number based on internal diameter
V_1, V_1'	functions defined in Appendix A
α	angle of incidence (in radians unless otherwise stated)
β	$\sqrt{M^2-1}$ $(= 3.84$ for $M = 3.97)$

REFERENCES

No.	Author	Title, etc
1	J. Seddon	The flow through short straight pipes in a compressible viscous stream. A.R.C. C.P. 355, April 1955
2	P.H. Cook	Supersonic wind tunnel measurements of the loads and internal pressure distributions on ducts at incidence. A.R.C. C.P. 768, February 1964
3	P.H. Cook	Supersonic wind tunnel measurements of the loads and internal pressure distributions on internally parallel ducts at incidence. A.R.C. 26291, May 1964
4	K.C. Moore J.G. Jones	Some aspects of the design of half-ring wing-body combinations with prescribed wing loadings. A.R.C. 24726, December 1962
5	D.R. Andrews C.S. Brown	Calibration of the flow in the Mach 4 working section of the 4 ft by 3 ft HSST at R.A.E. Bedford. A.R.C. 24279, May 1962
6	G.N. Ward	The approximate external and internal flow past a quasi-cylindrical tube moving at supersonic speeds. Q. Jl. Mech. Appl.Math. 1, pp 225-45, 1948
7	G.N. Ward	Linearised theory of steady high speed flow. Cambridge Univ. Press, 1955
8	M.J. Lighthill	Supersonic flow past bodies of revolution. ARC R&M No.2003, January 1945

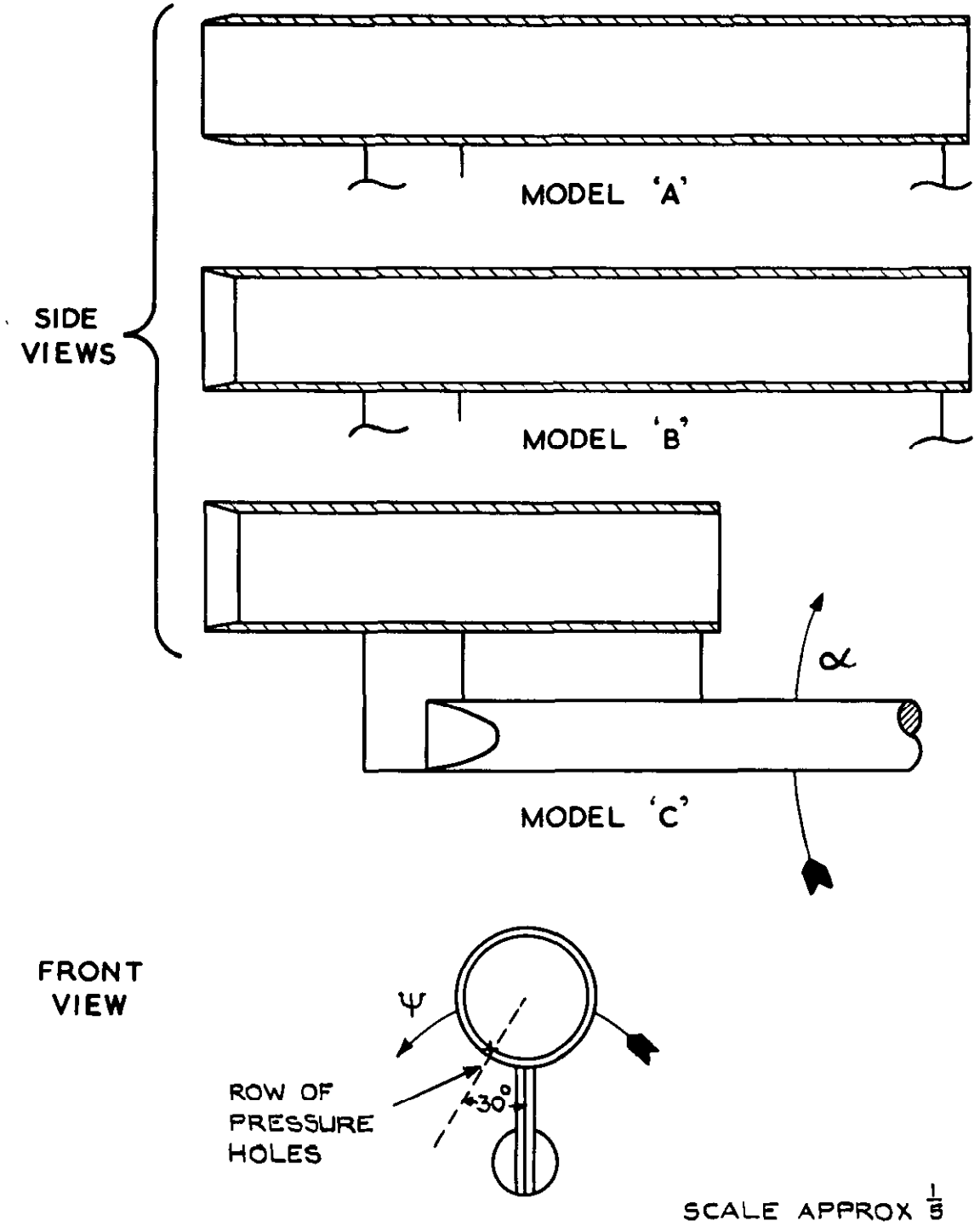

FIG. 1 MODELS TESTED

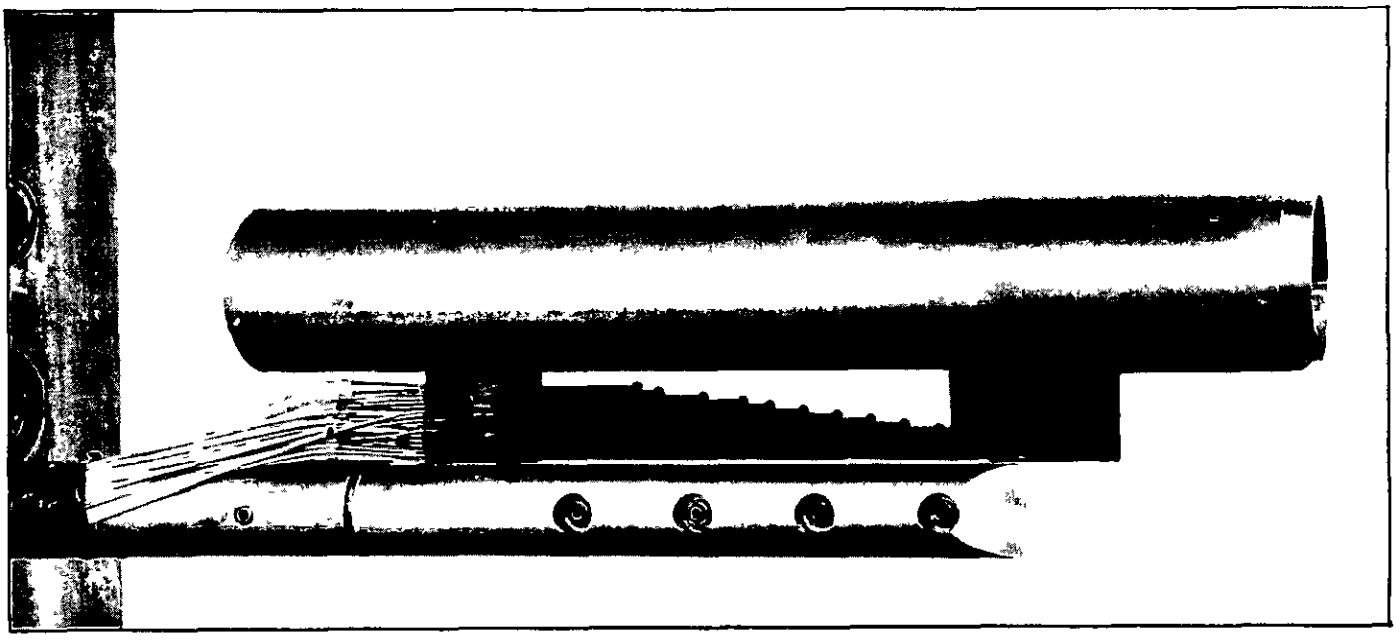

Fig.2 Model 'A', showing support sting,pylon, and pressure tubing

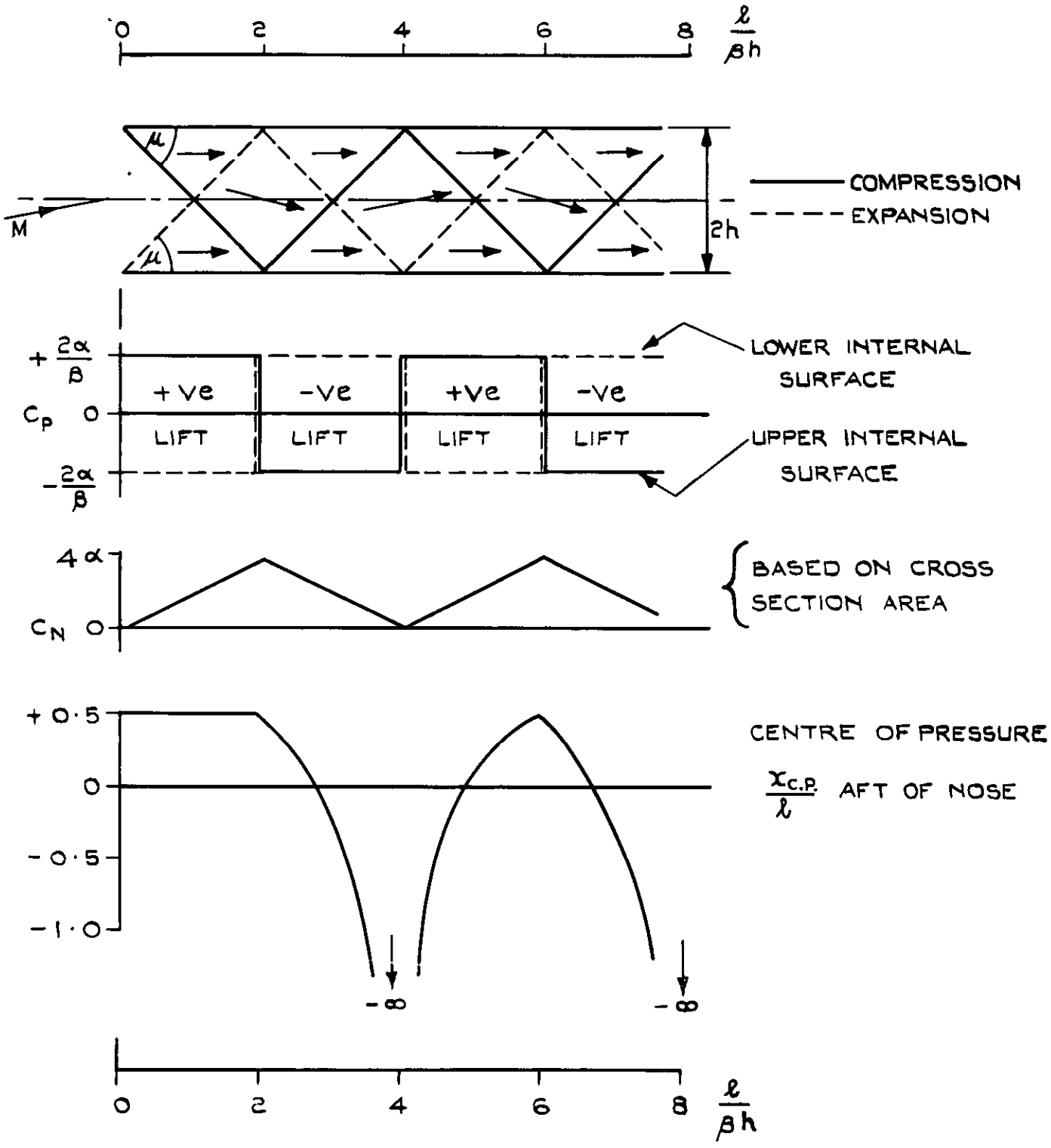

FIG. 3 LINEAR THEORY SOLUTION FOR FLOW THROUGH A RECTANGULAR DUCT (FROM REF. 2)

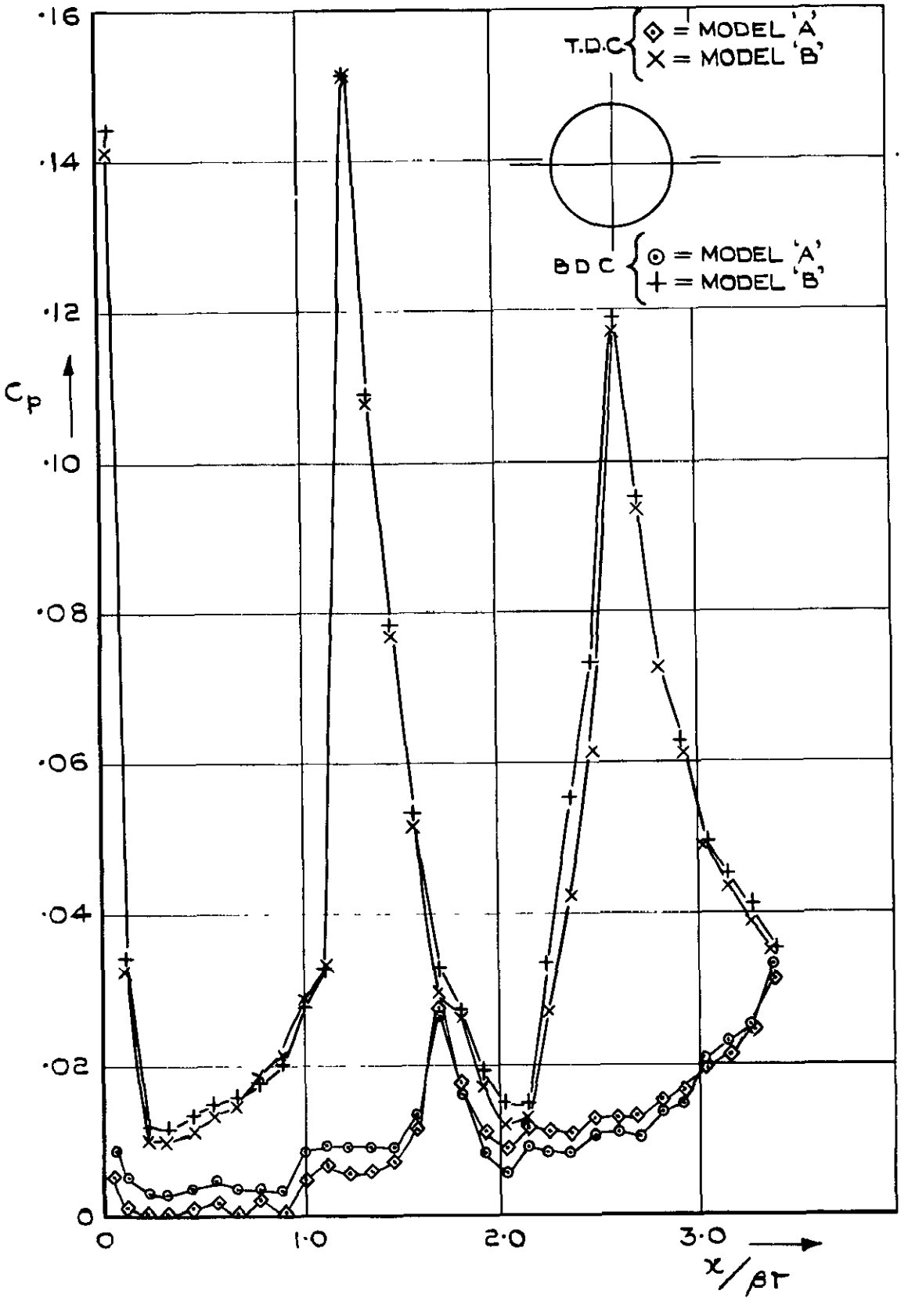

FIG.4 PRESSURE DISTRIBUTIONS AT ZERO INCIDENCE FOR MODELS 'A' AND 'B'

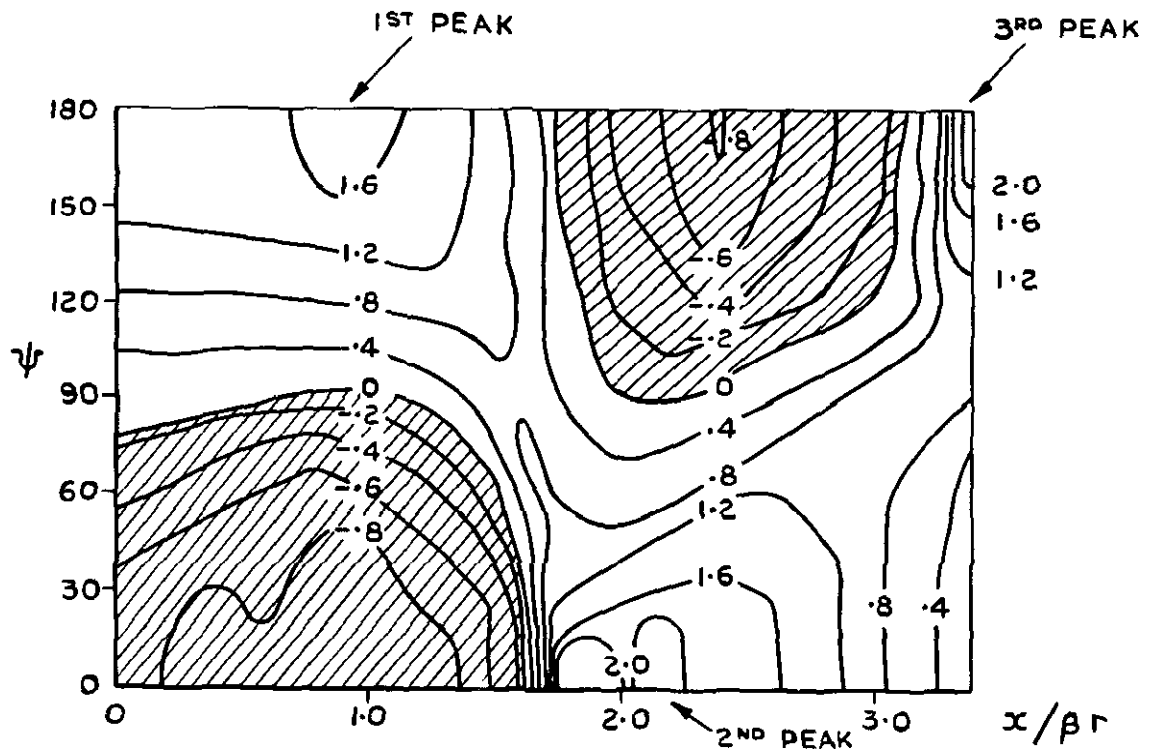

FIG.5 PRESSURE CONTOURS FOR MODEL 'A'

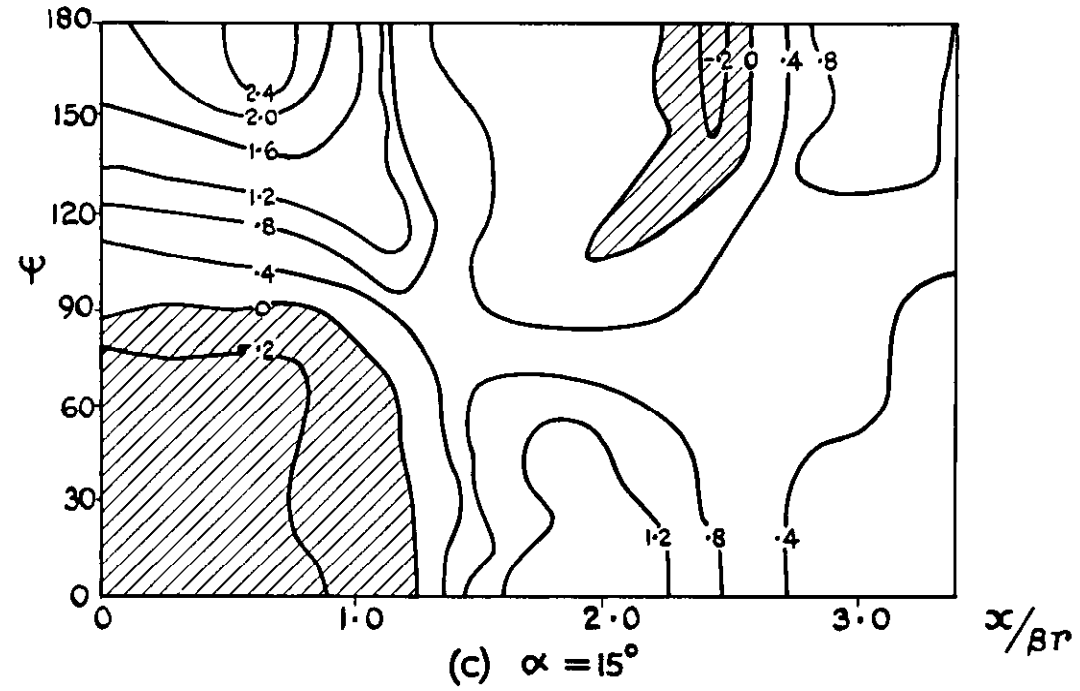

(c) $\alpha = 15°$

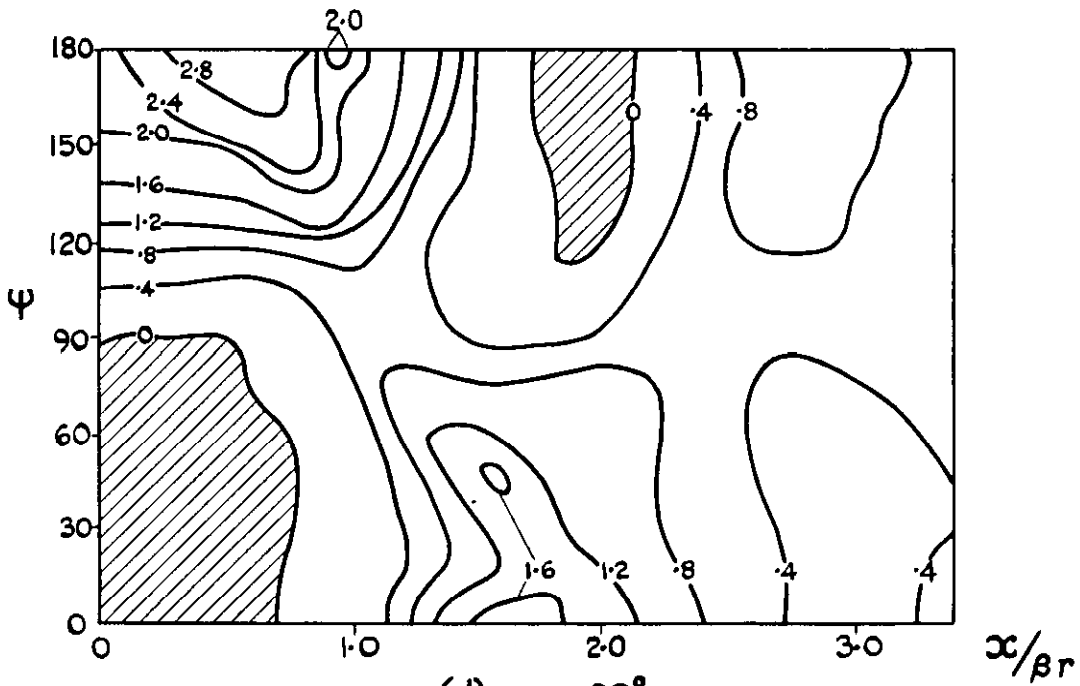

(d) $\alpha = 20°$

FIG. 5 (CONCLD)

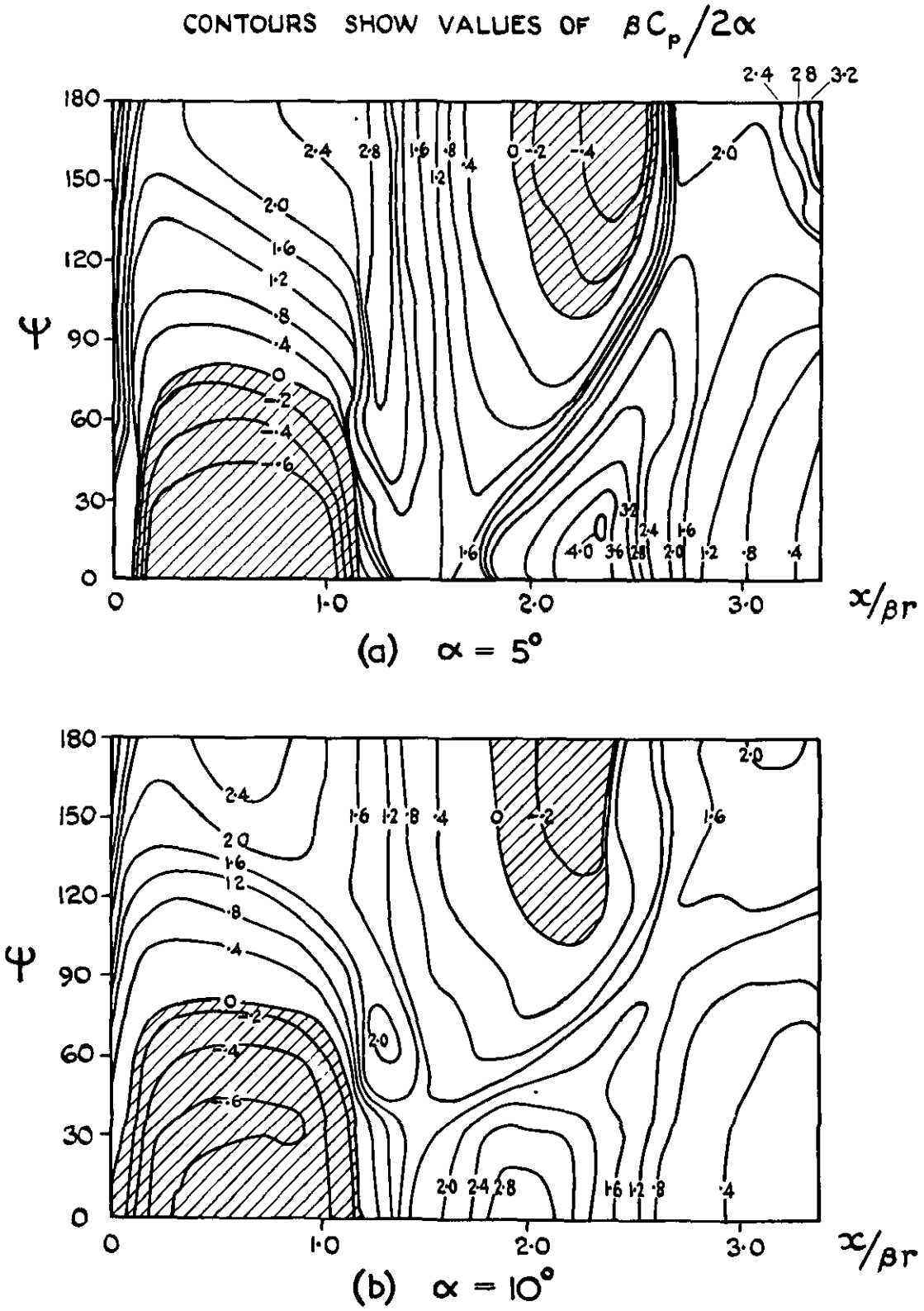

FIG.6 PRESSURE CONTOURS FOR MODEL "B"

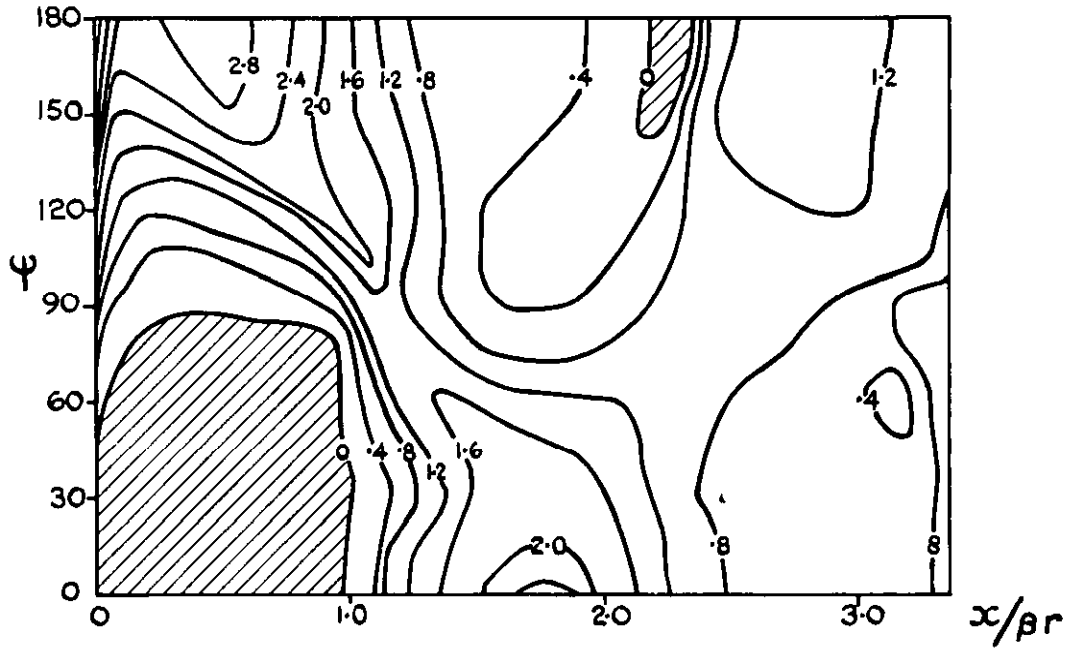

(c) $\alpha = 15°$

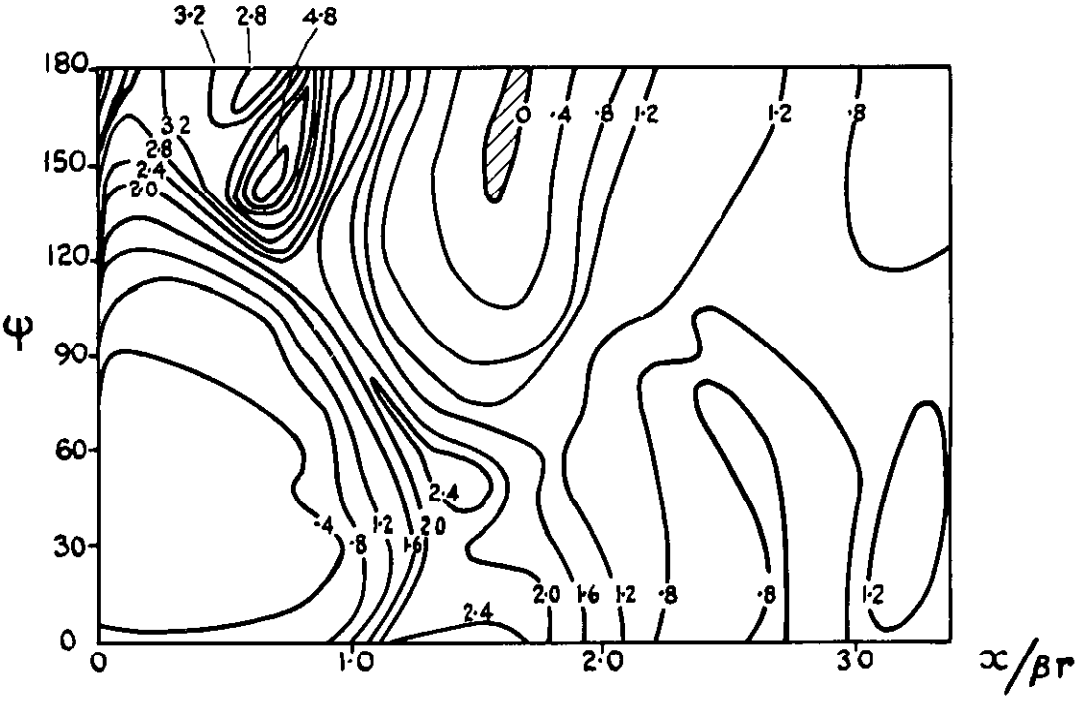

(d) $\alpha = 20°$

FIG. 6 (CONCLD)

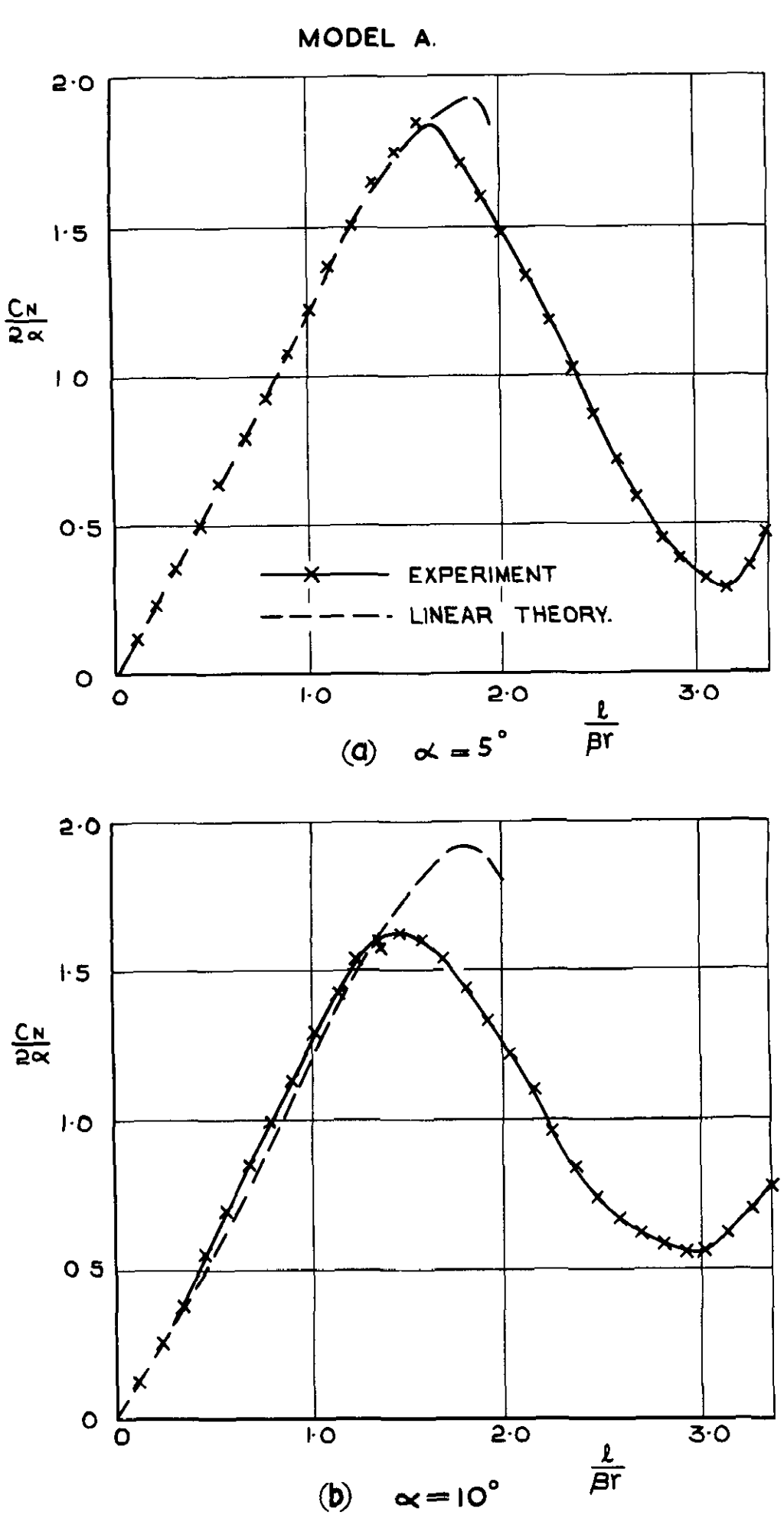

FIG. 7 NORMAL FORCE vs DUCT LENGTH FOR MODEL 'A'.

MODEL A.

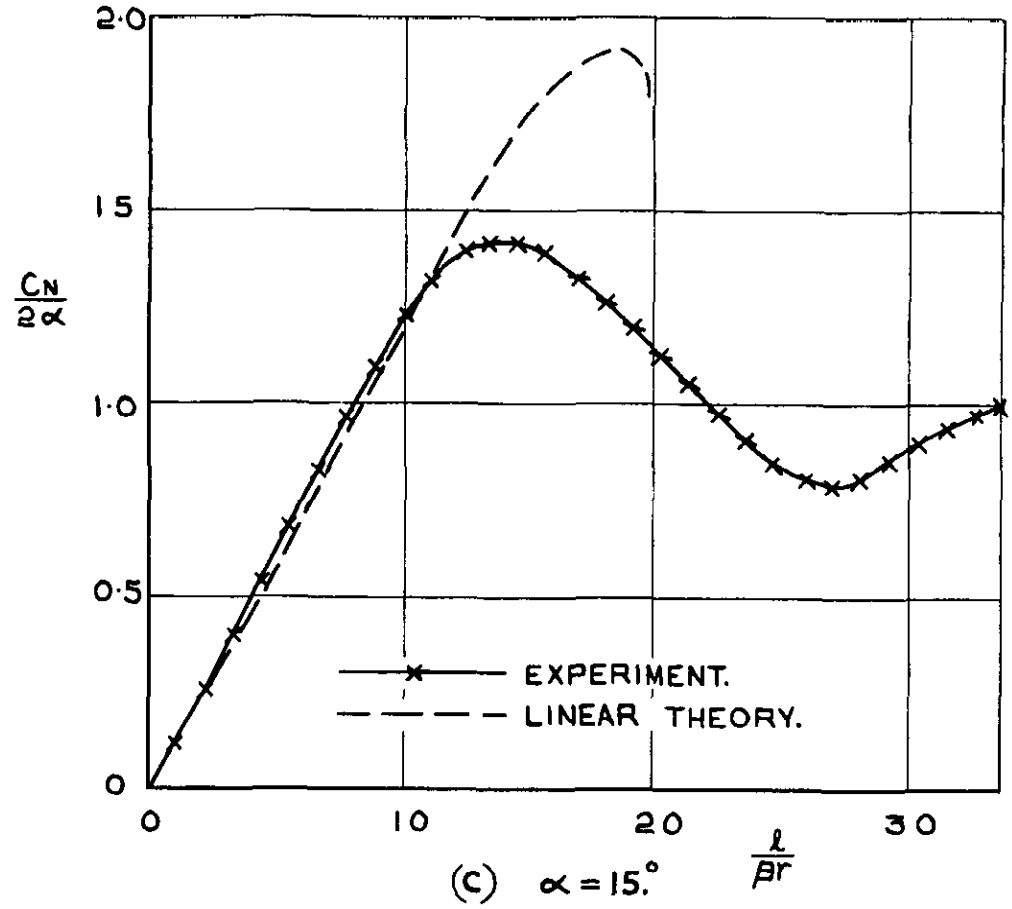

(c) $\alpha = 15.^\circ$

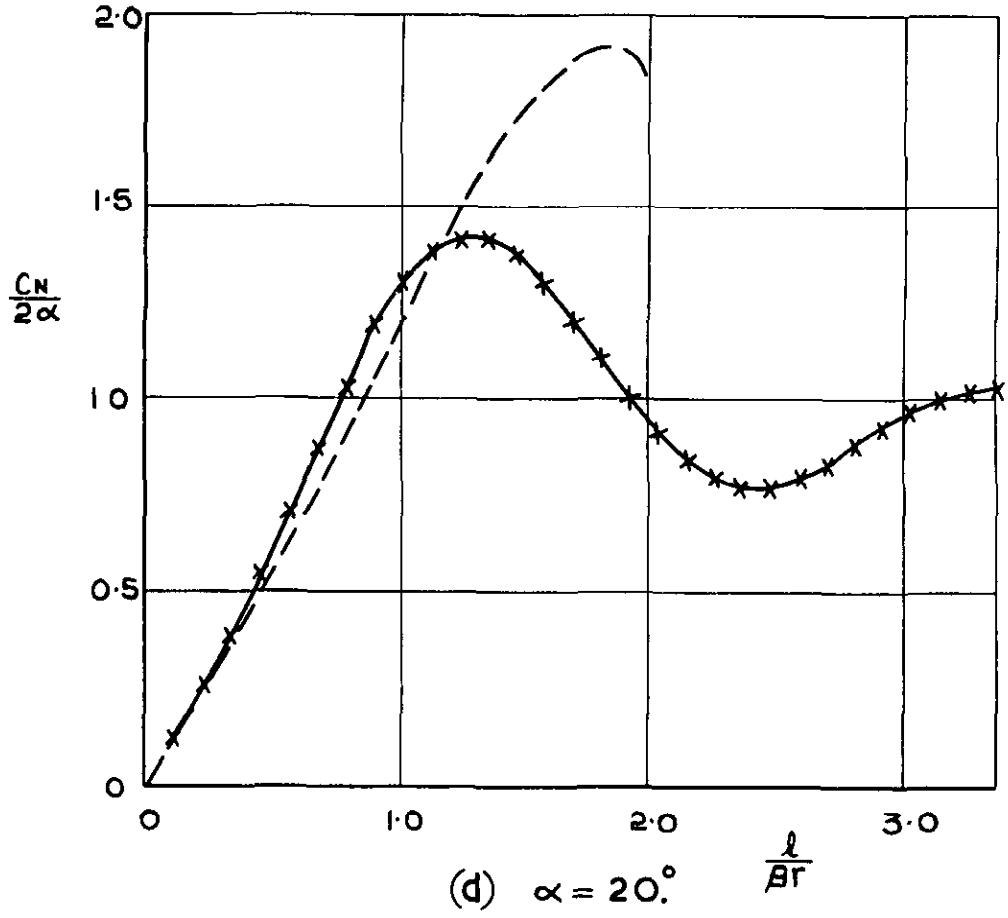

(d) $\alpha = 20.^\circ$

FIG. 7 (CONCLD.)

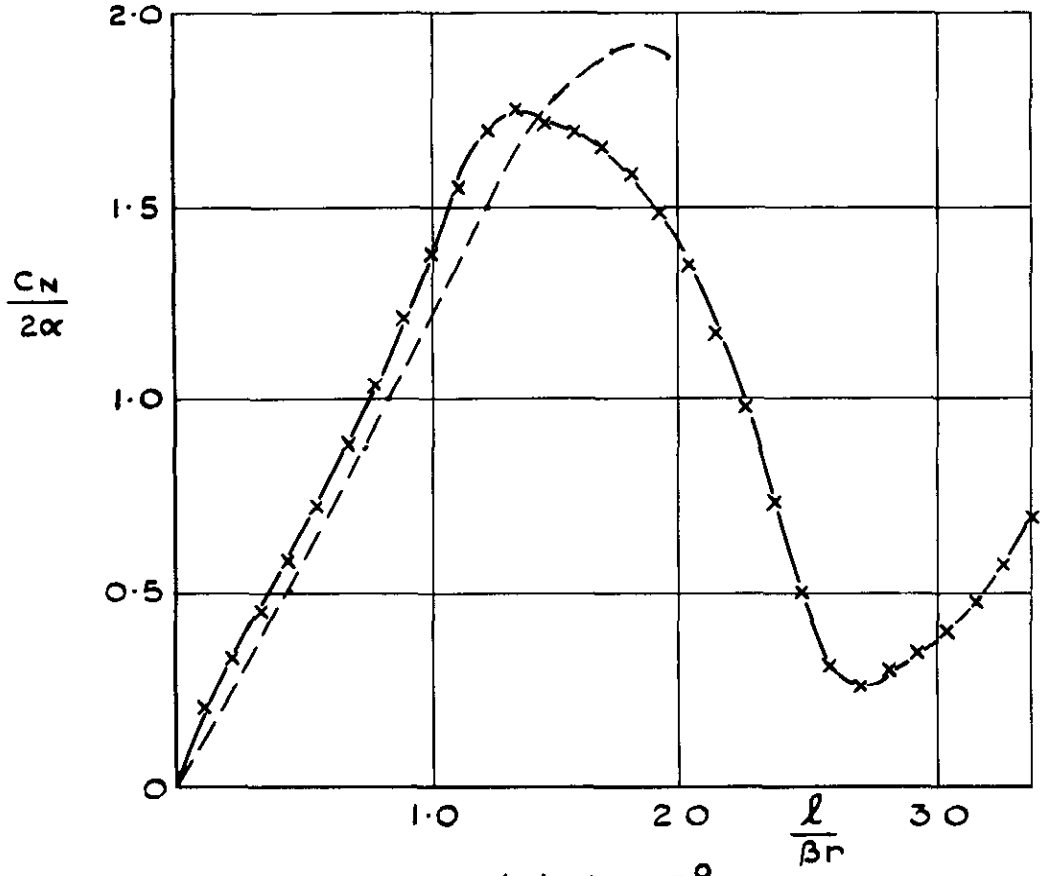

(a) $\alpha = 5°$

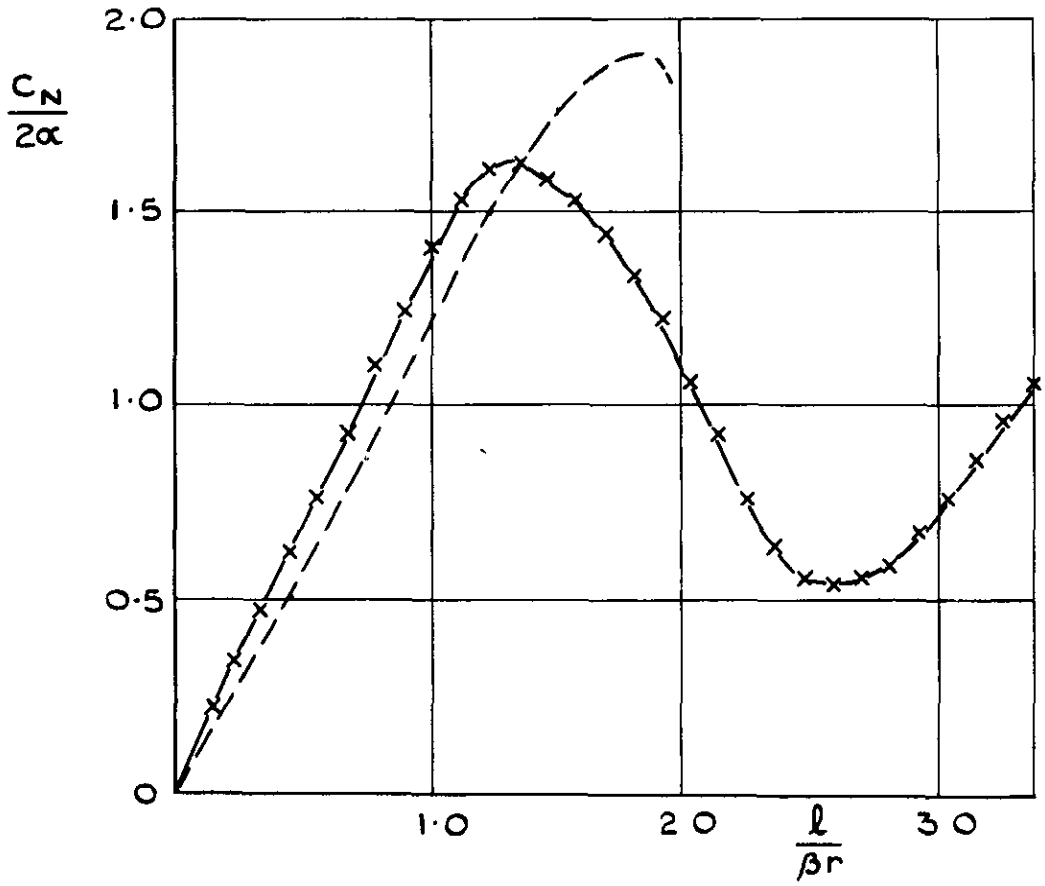

(b) $\alpha = 10°$

FIG.8 NORMAL FORCE vs DUCT LENGTH FOR MODEL 'B'

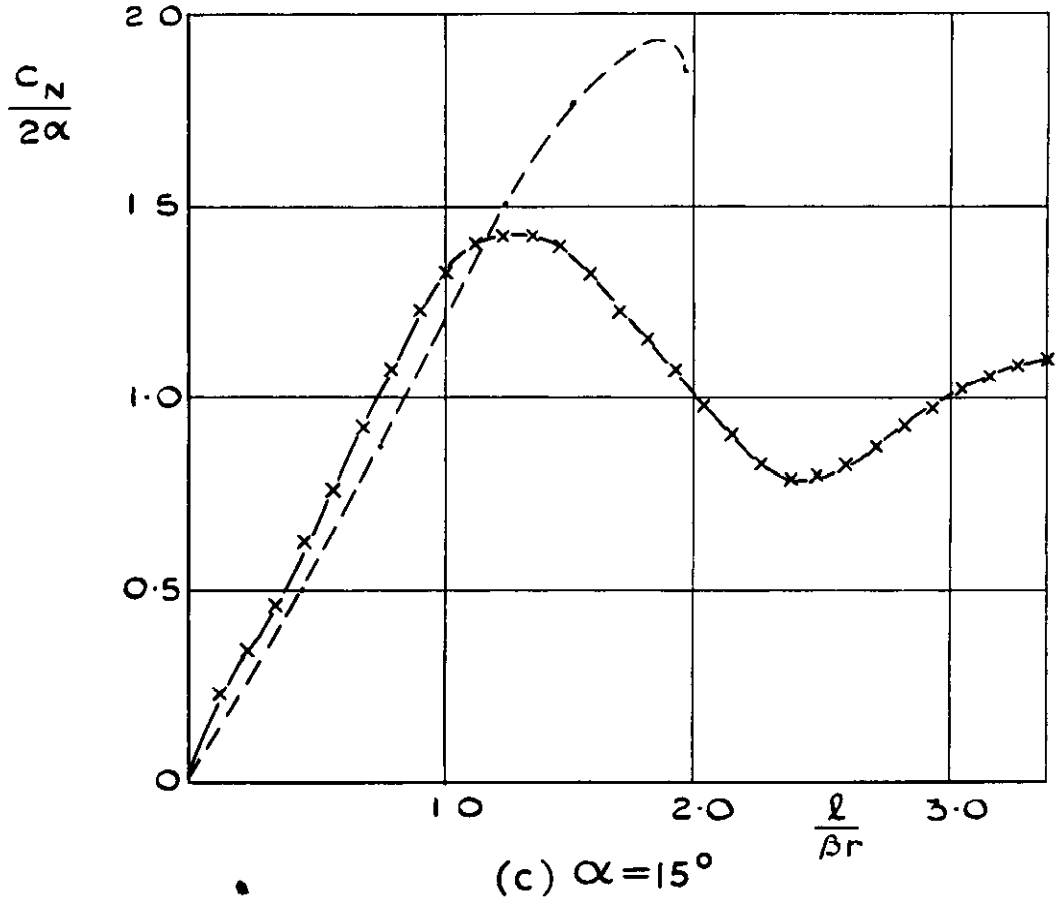

(c) $\alpha = 15°$

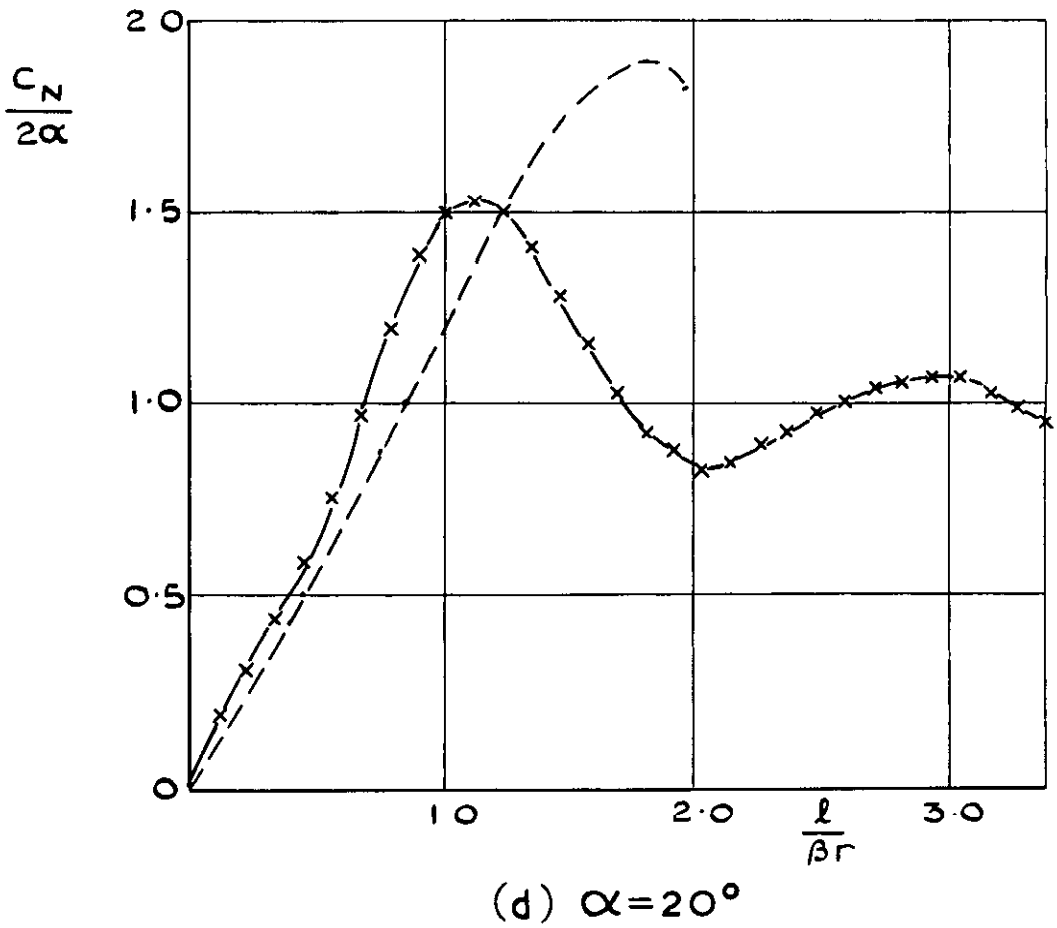

(d) $\alpha = 20°$

FIG. 8 (CONCLD.)

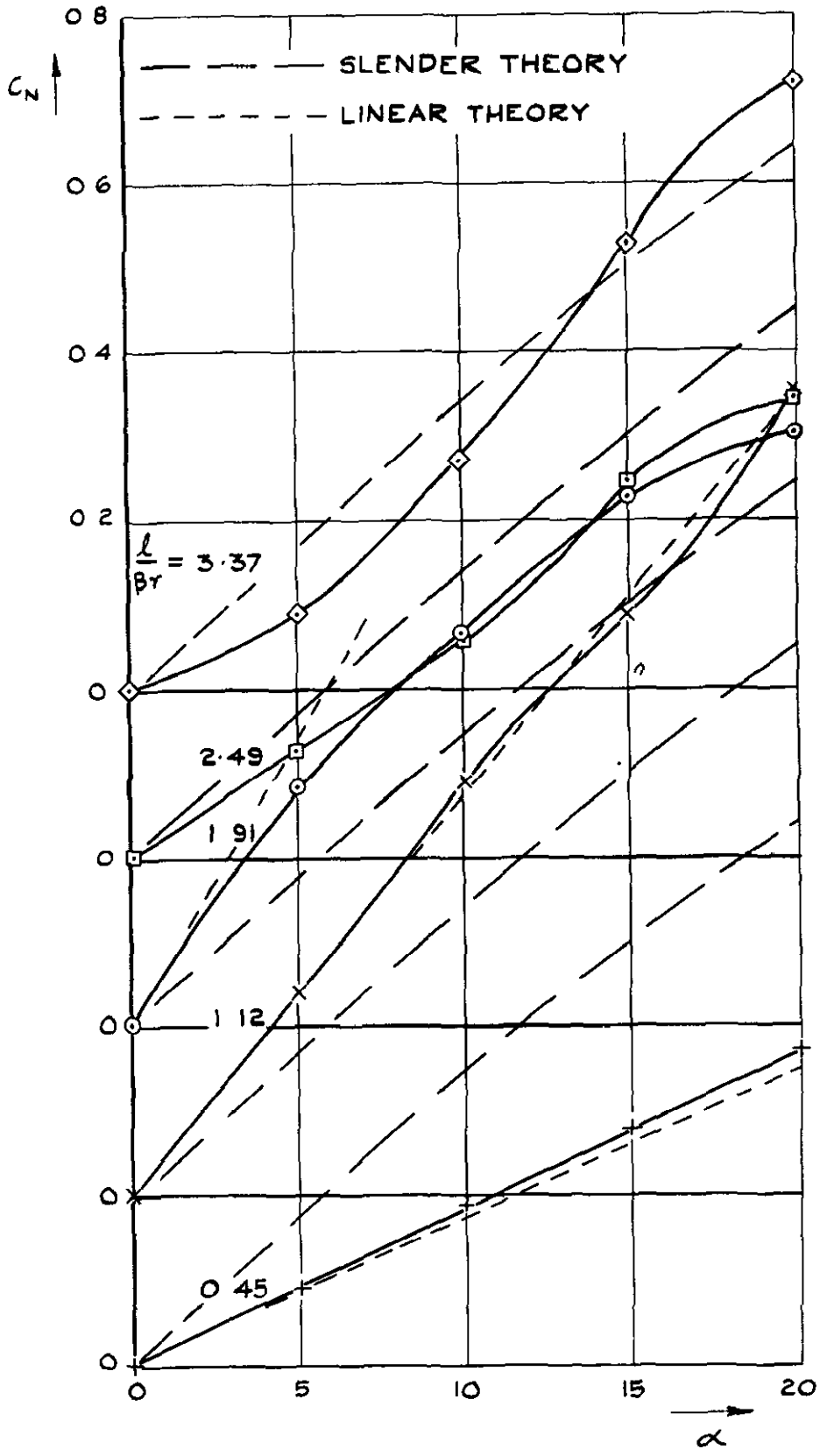

FIG. 9 VARIATION OF NORMAL FORCE WITH INCIDENCE FOR TUBES OF VARIOUS LENGTHS (MODEL 'A')

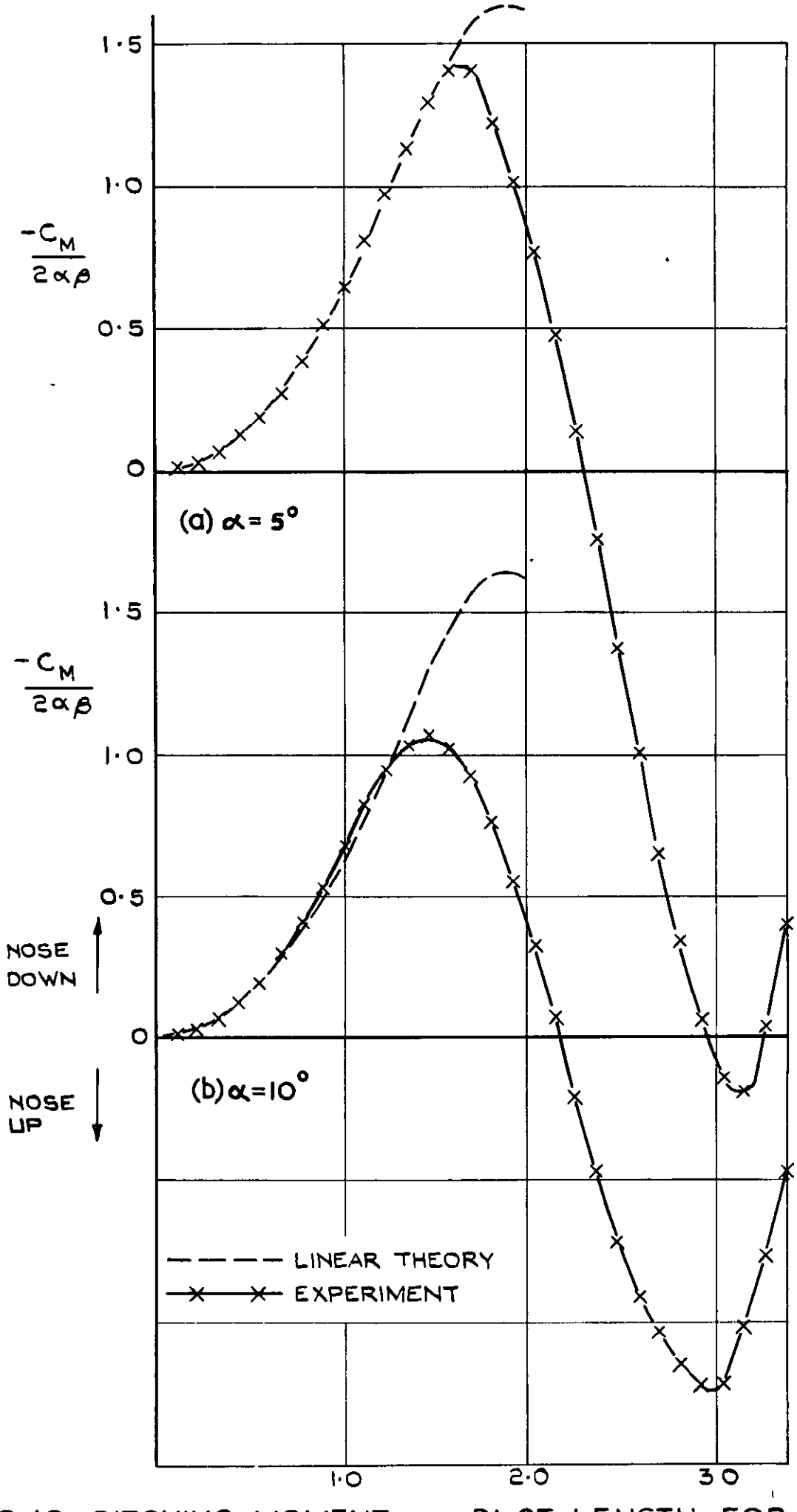

FIG. 10 PITCHING MOMENT VS DUCT LENGTH FOR MODEL 'A'

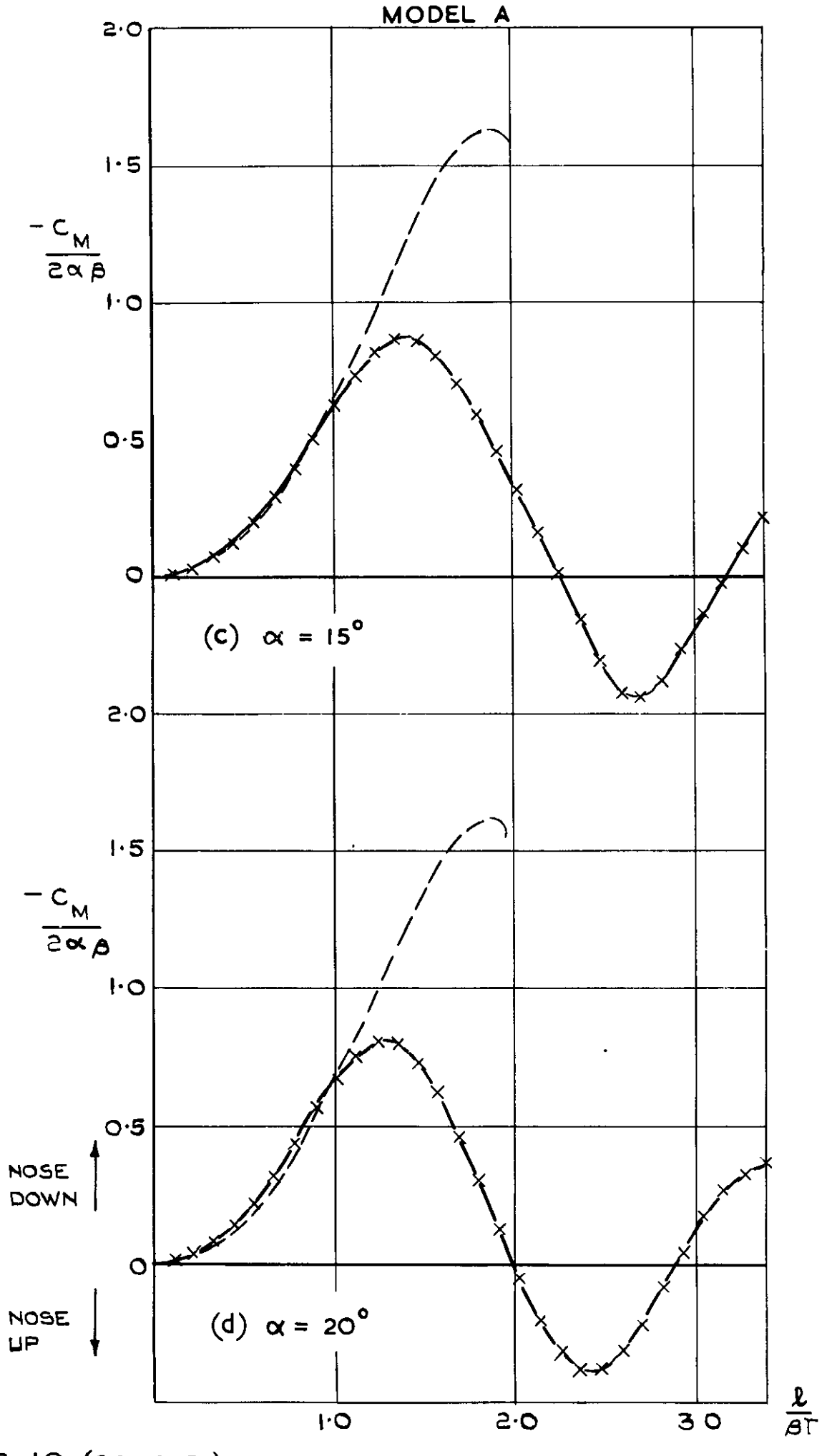

FIG. 10 (CONCLD)

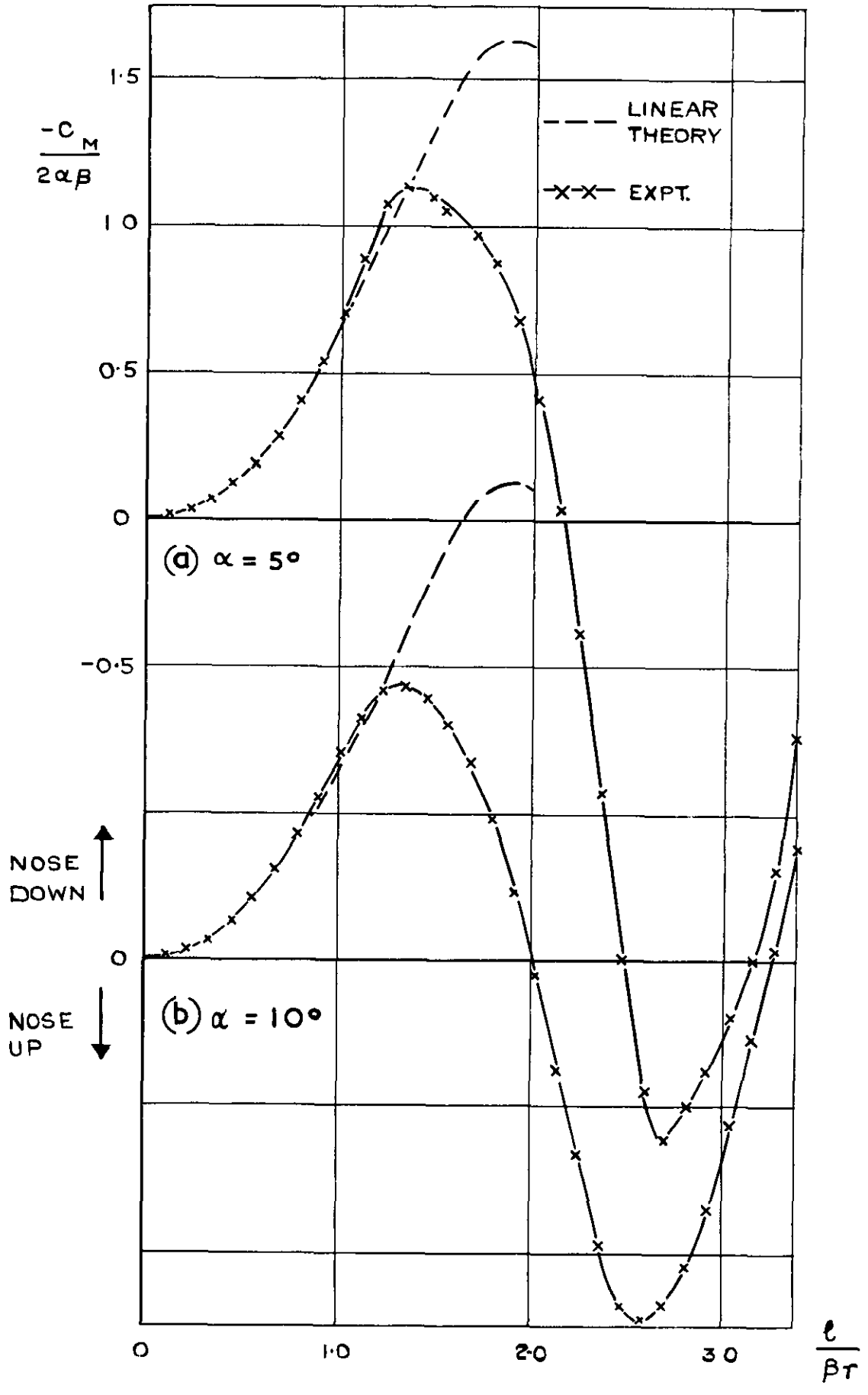

FIG. 11 PITCHING MOMENT VS. DUCT LENGTH FOR MODEL 'B'

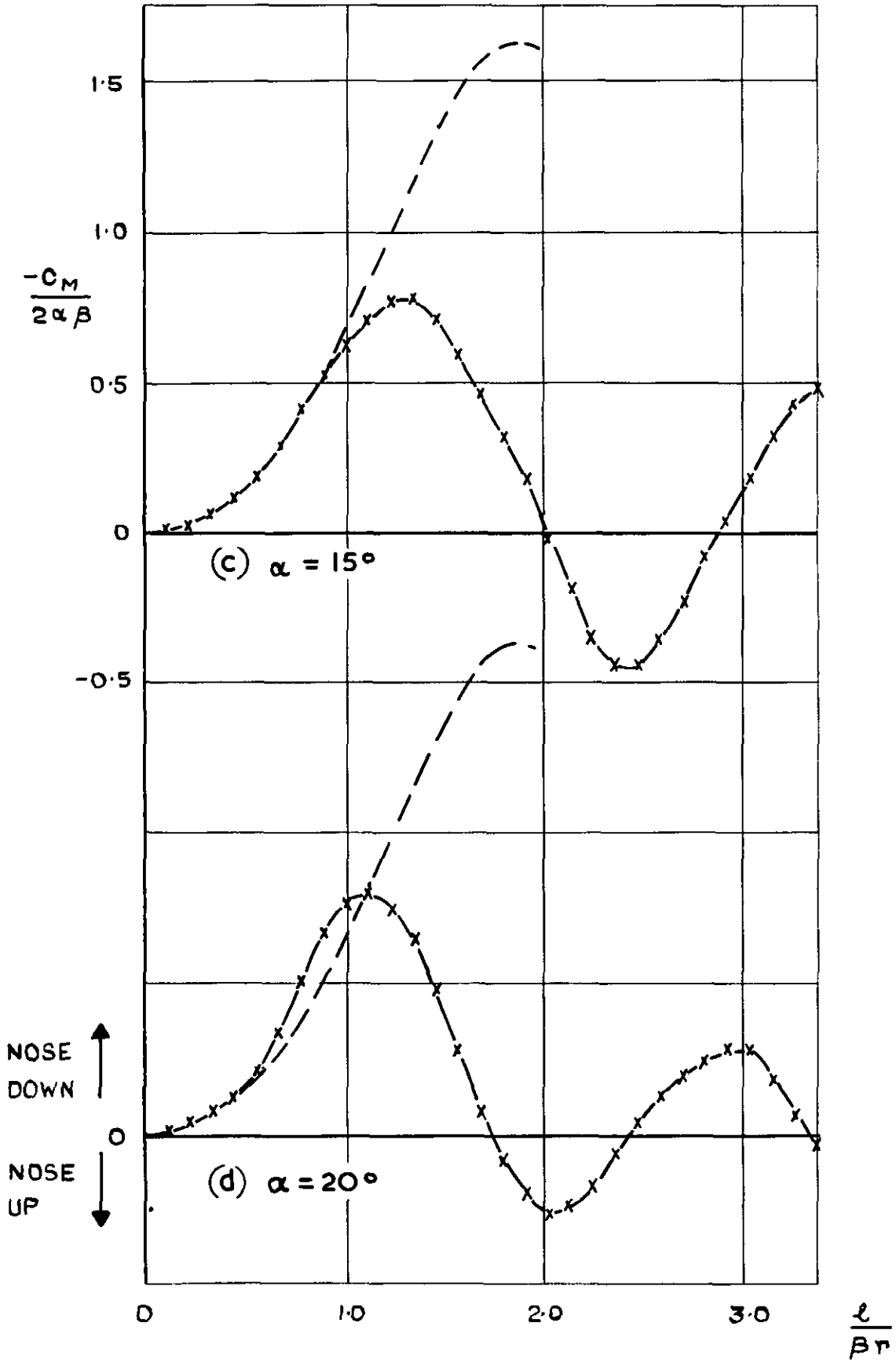

FIG. 11 (CONCLD.)

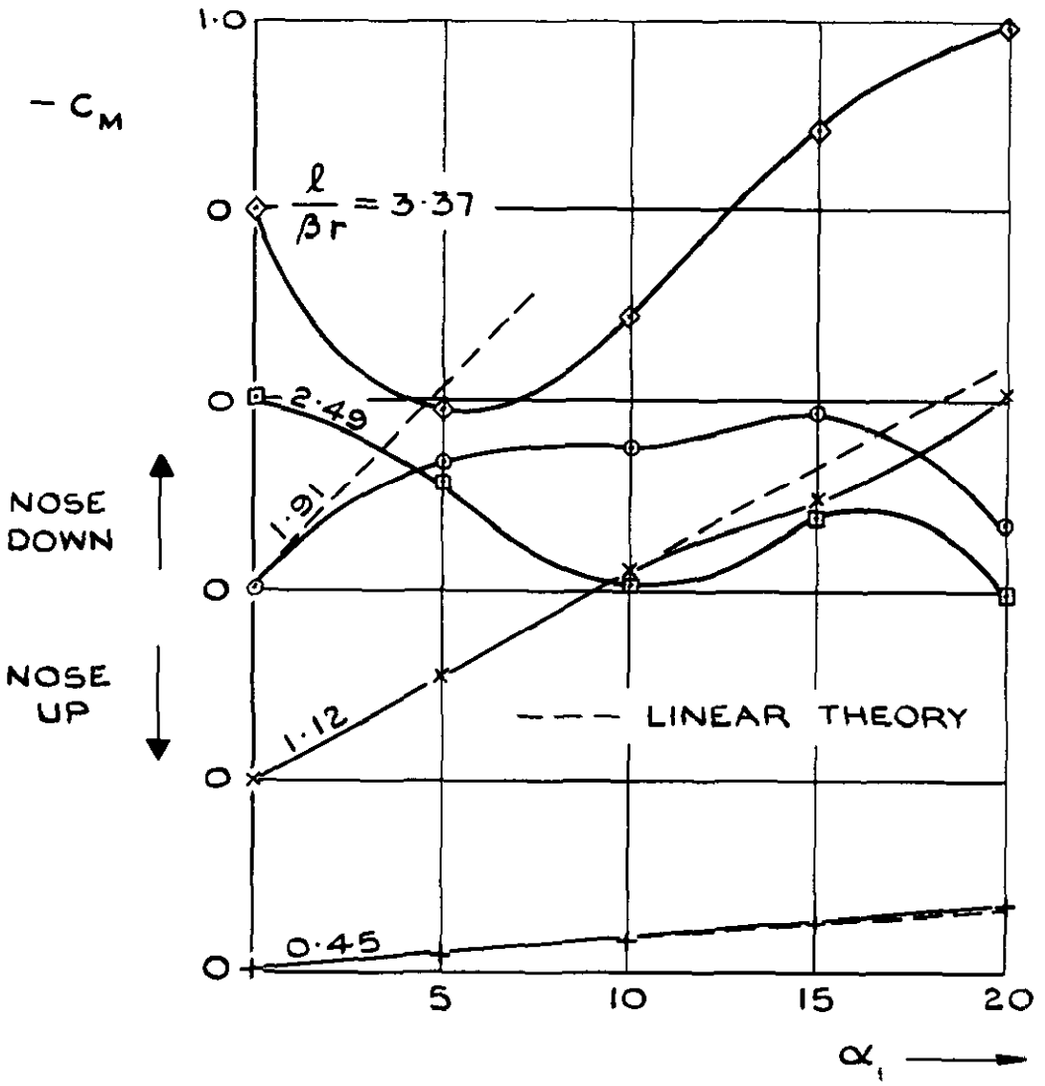

FIG.12 VARIATION OF PITCHING MOMENT WITH INCIDENCE FOR TUBES OF VARIOUS LENGTHS (MODEL 'A')

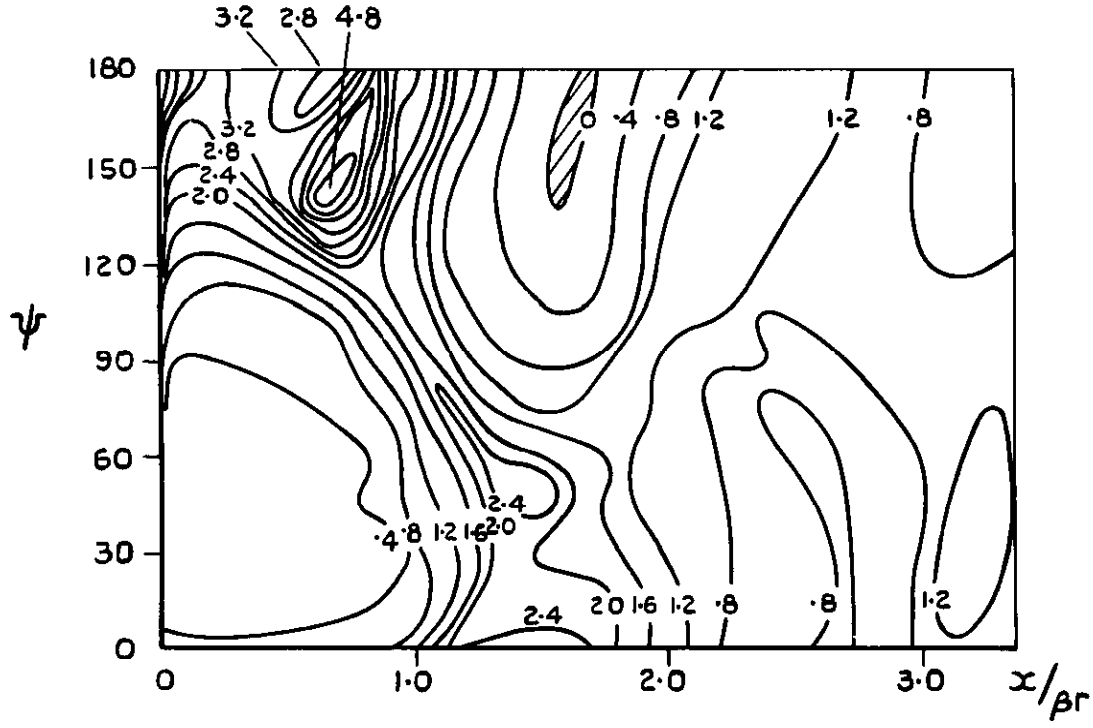

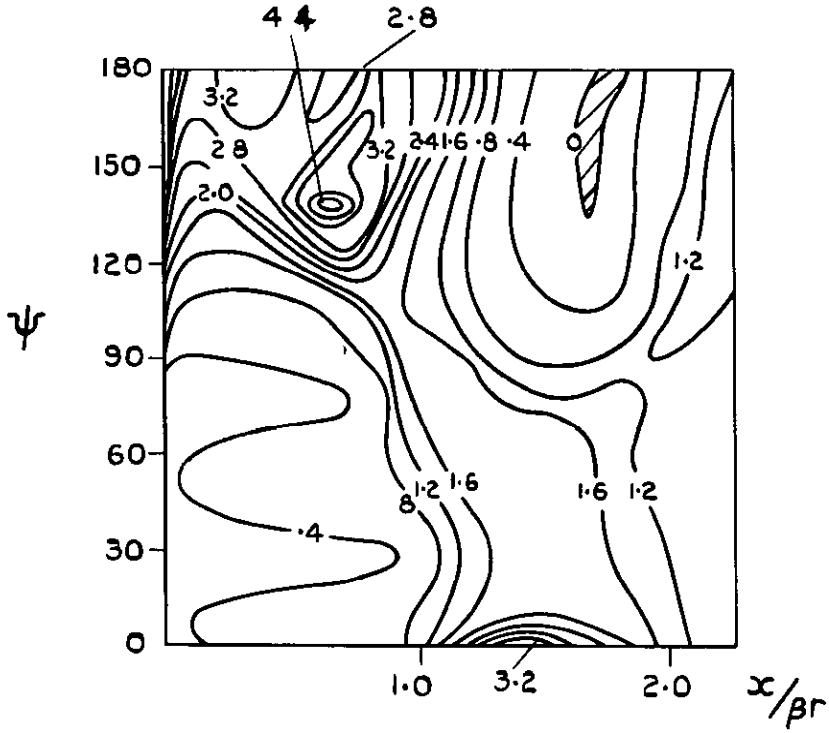

FIG. 13 COMPARISON OF PRESSURE CONTOURS AT $\alpha = 20^{\circ}$, MODELS "B" AND "C"

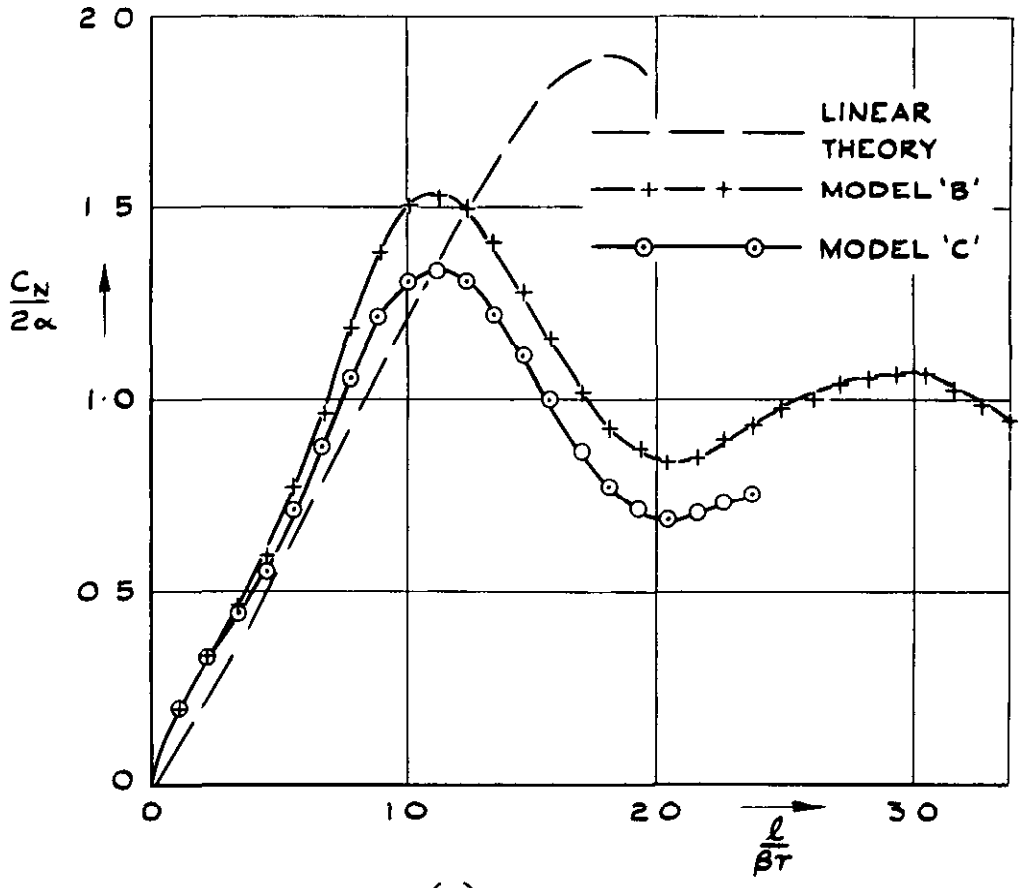

(a) $\alpha = 20°$

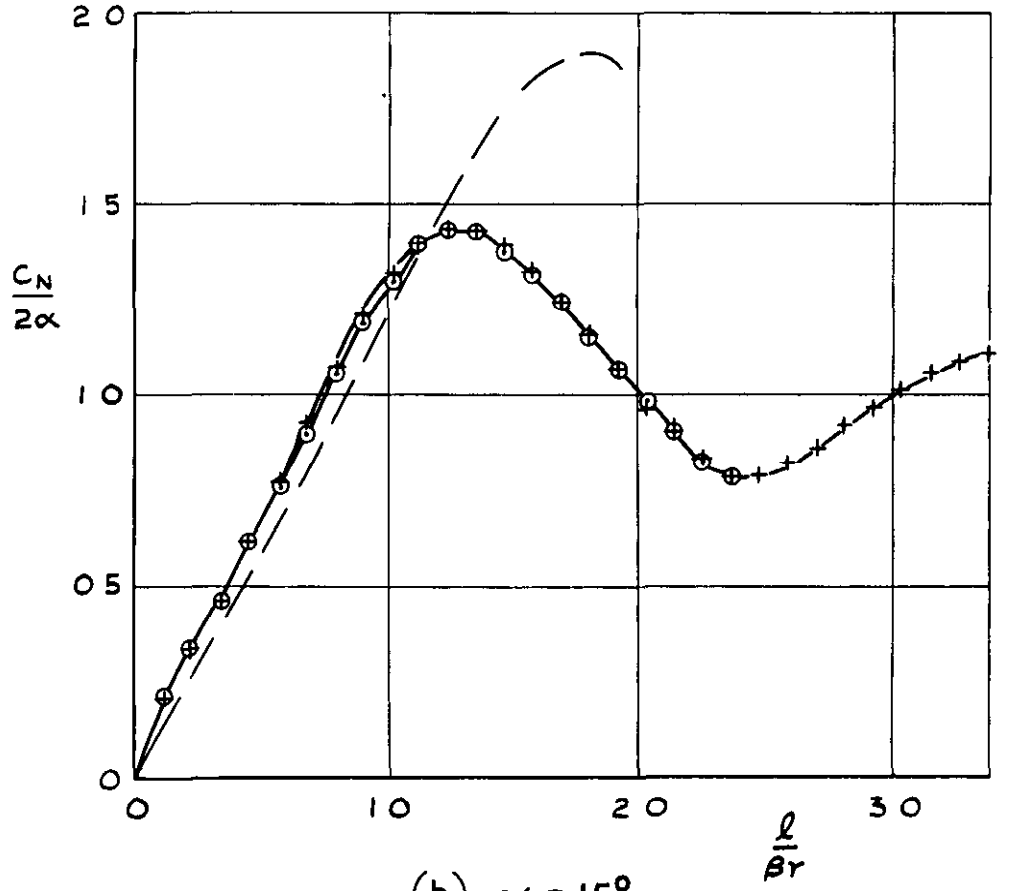

(b) $\alpha = 15°$

FIG. 14 (a & b) NORMAL FORCE RESULTS OBTAINED FROM MODELS "B" AND "C"

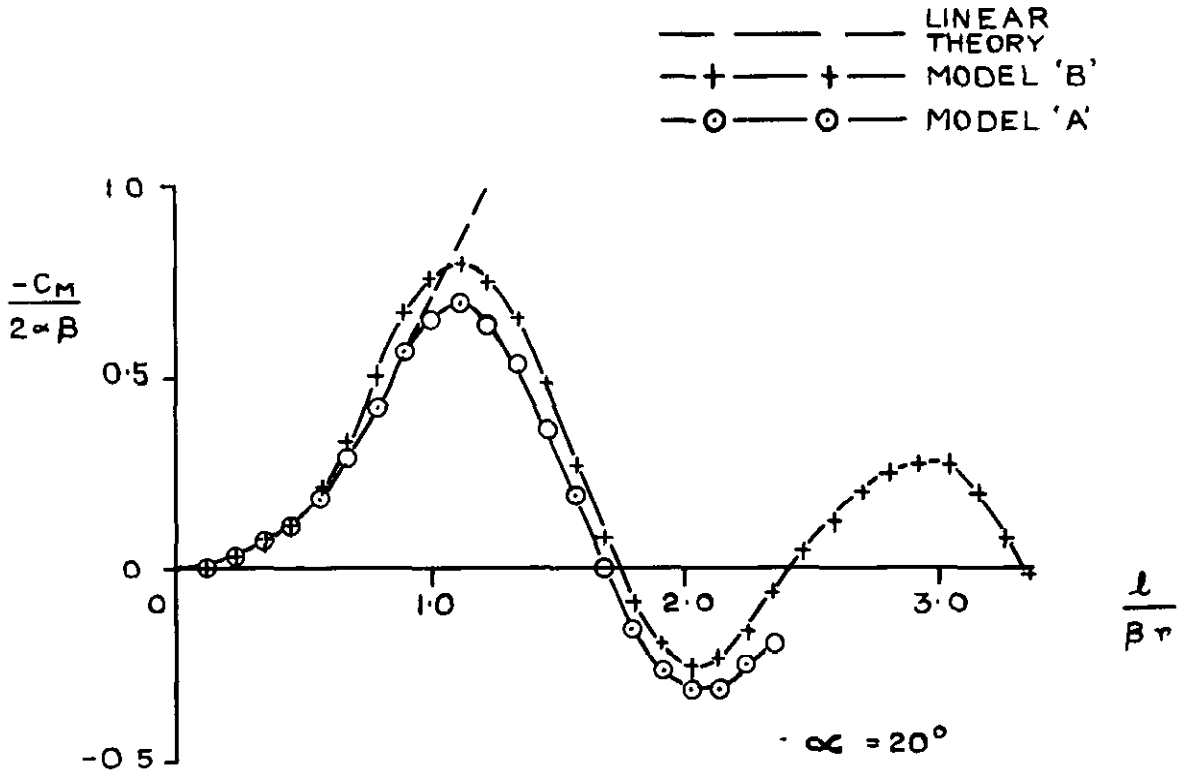

FIG.15 PITCHING MOMENT RESULTS OBTAINED FROM MODELS 'B' AND 'C'

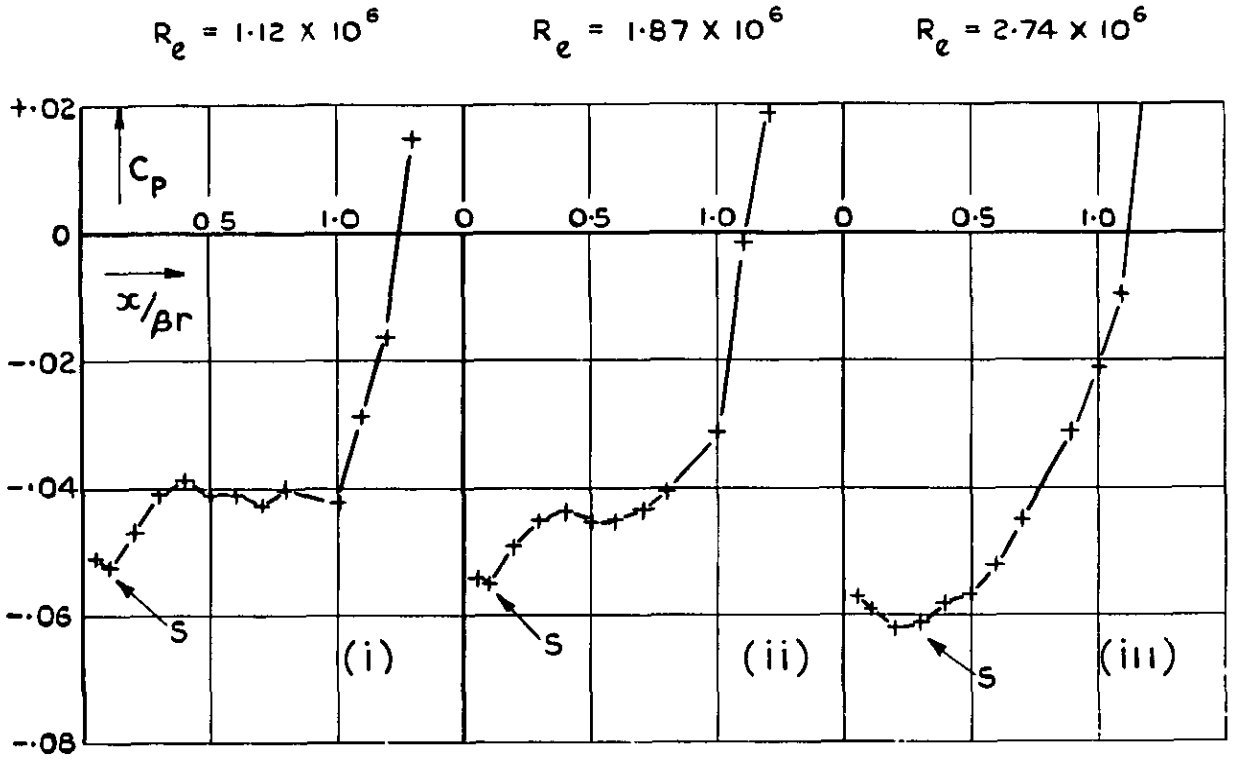

(a) INCREASING INCIDENCE

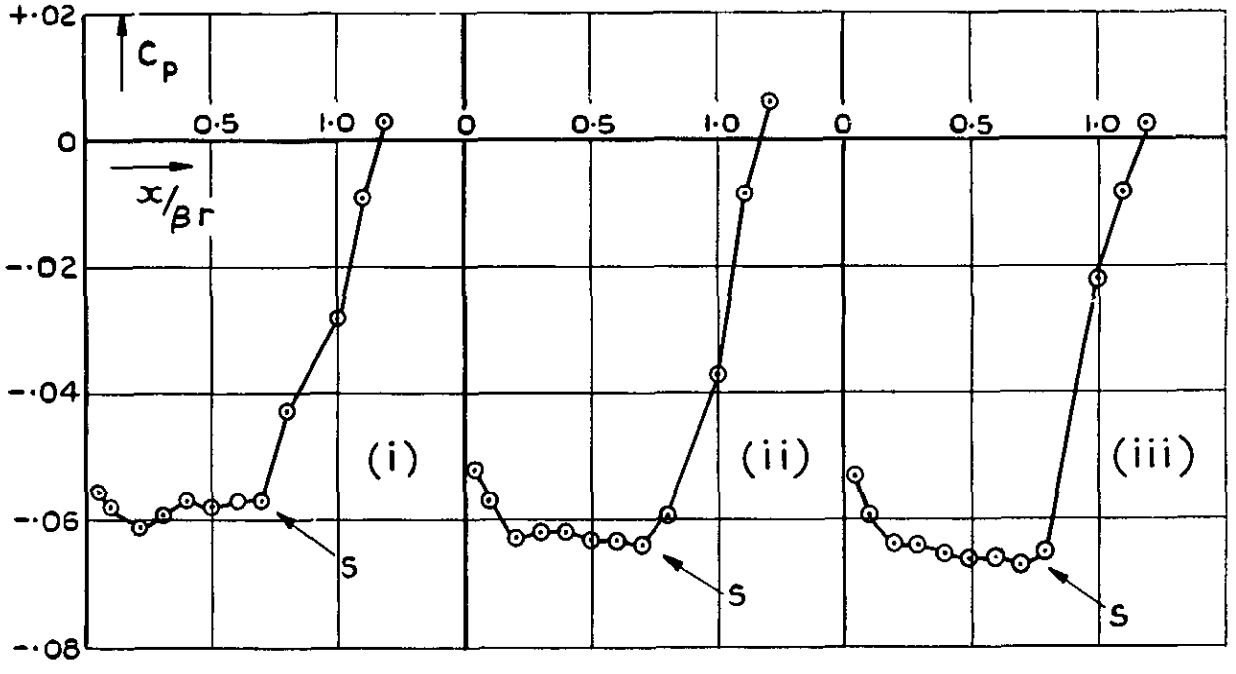

(b) DECREASING INCIDENCE

FIG.16 PRESSURE DISTRIBUTIONS ALONG $\psi = 0$ AT $\alpha = 10^\circ$ (MODEL 'A')

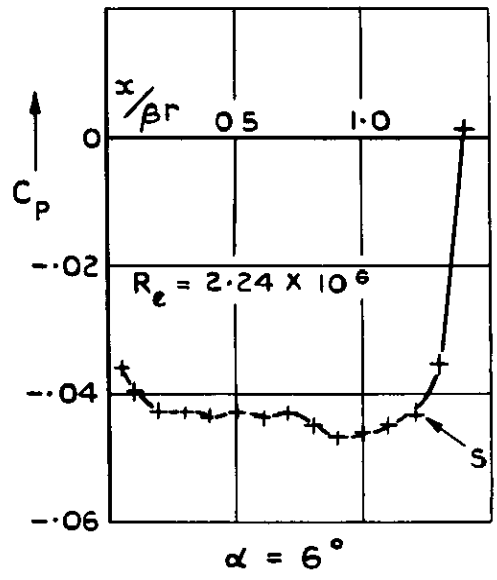

FIG.17 TYPICAL PRESSURE DISTRIBUTION ALONG ψ=O AT INCIDENCE BELOW HYSTERESIS RANGE (MODEL 'A')

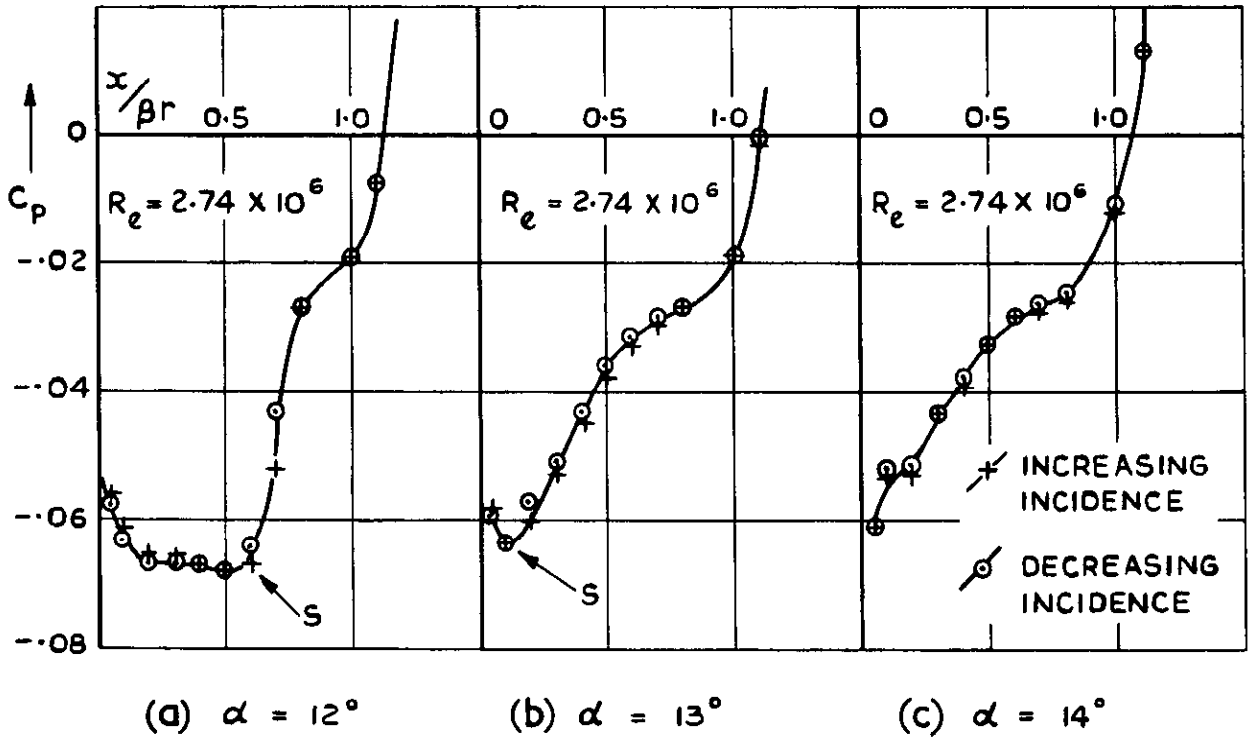

FIG. 18 PRESSURE DISTRIBUTIONS ALONG ψ = O AT INCIDENCES ABOVE HYSTERESIS RANGE (MODEL 'A')

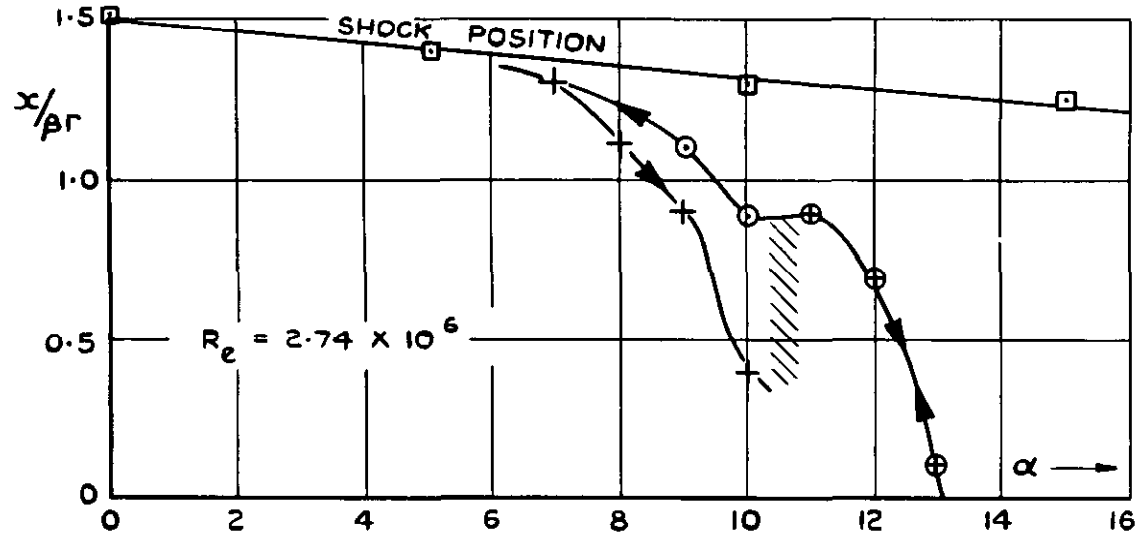

(a)

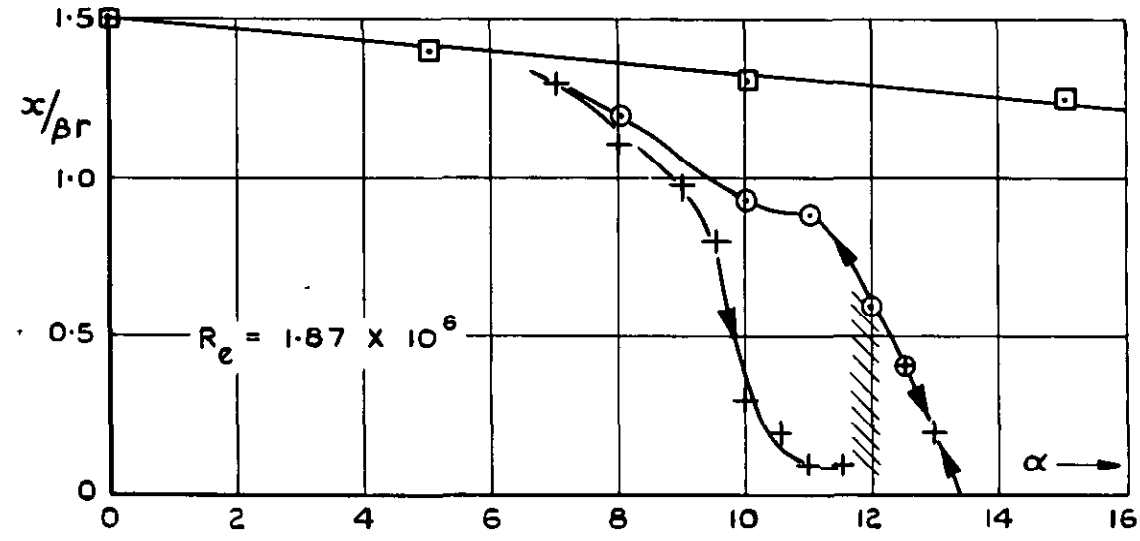

(b)

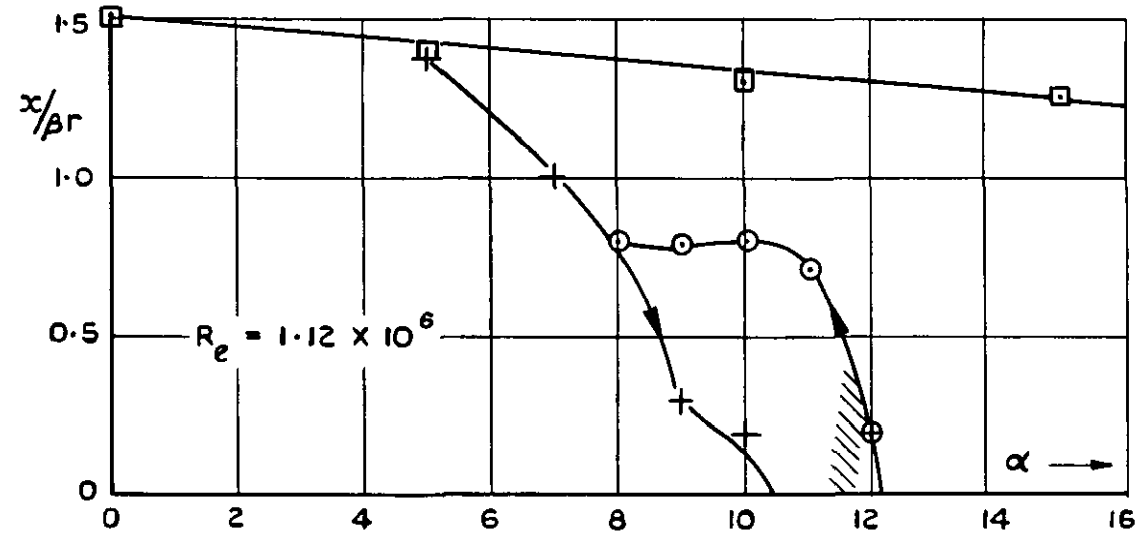

(c)

FIG. 19 POSITION OF SEPARATION POINT

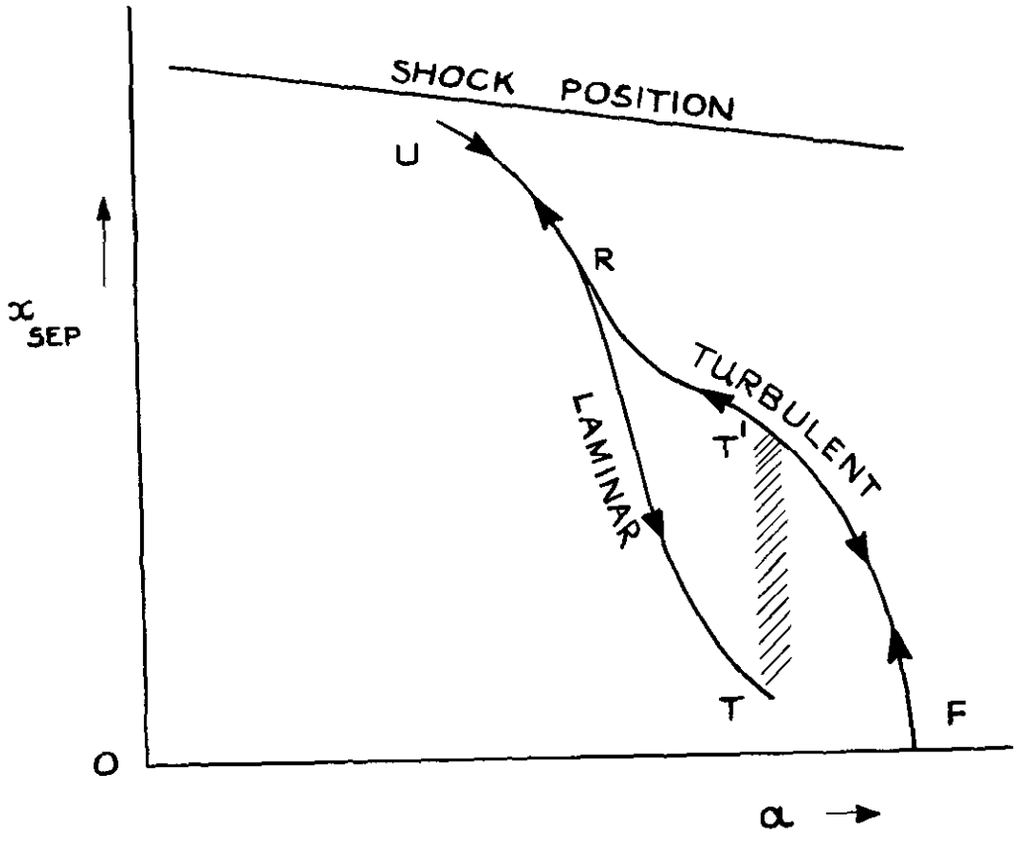

FIG 20 POSITION OF SEPARATION POINT
(DIAGRAMMATIC)

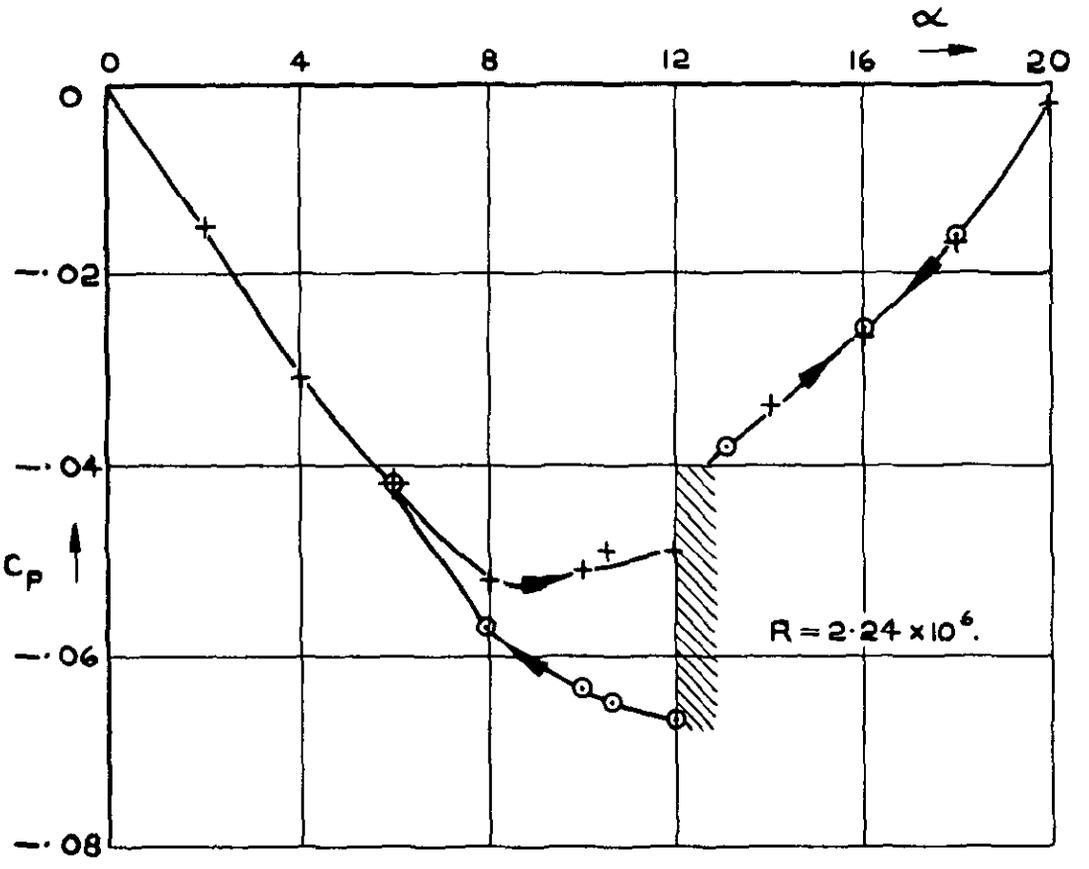

FIG.21 VARIATION OF C_p WITH α AT $x/\beta r = 0{\cdot}5$, $\psi = 0$.

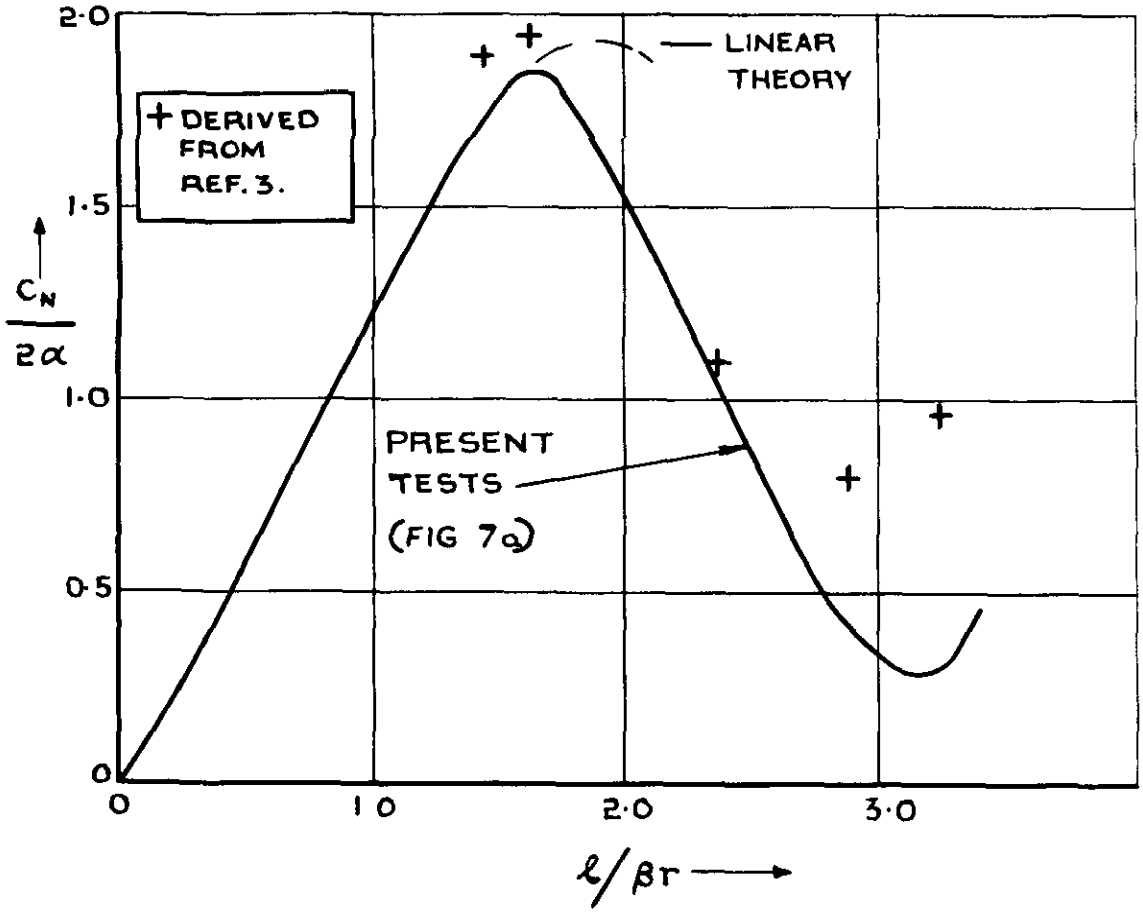

FIG 22. COMPARISON WITH RESULTS OF REF 3.
(AT SMALL INCIDENCE)

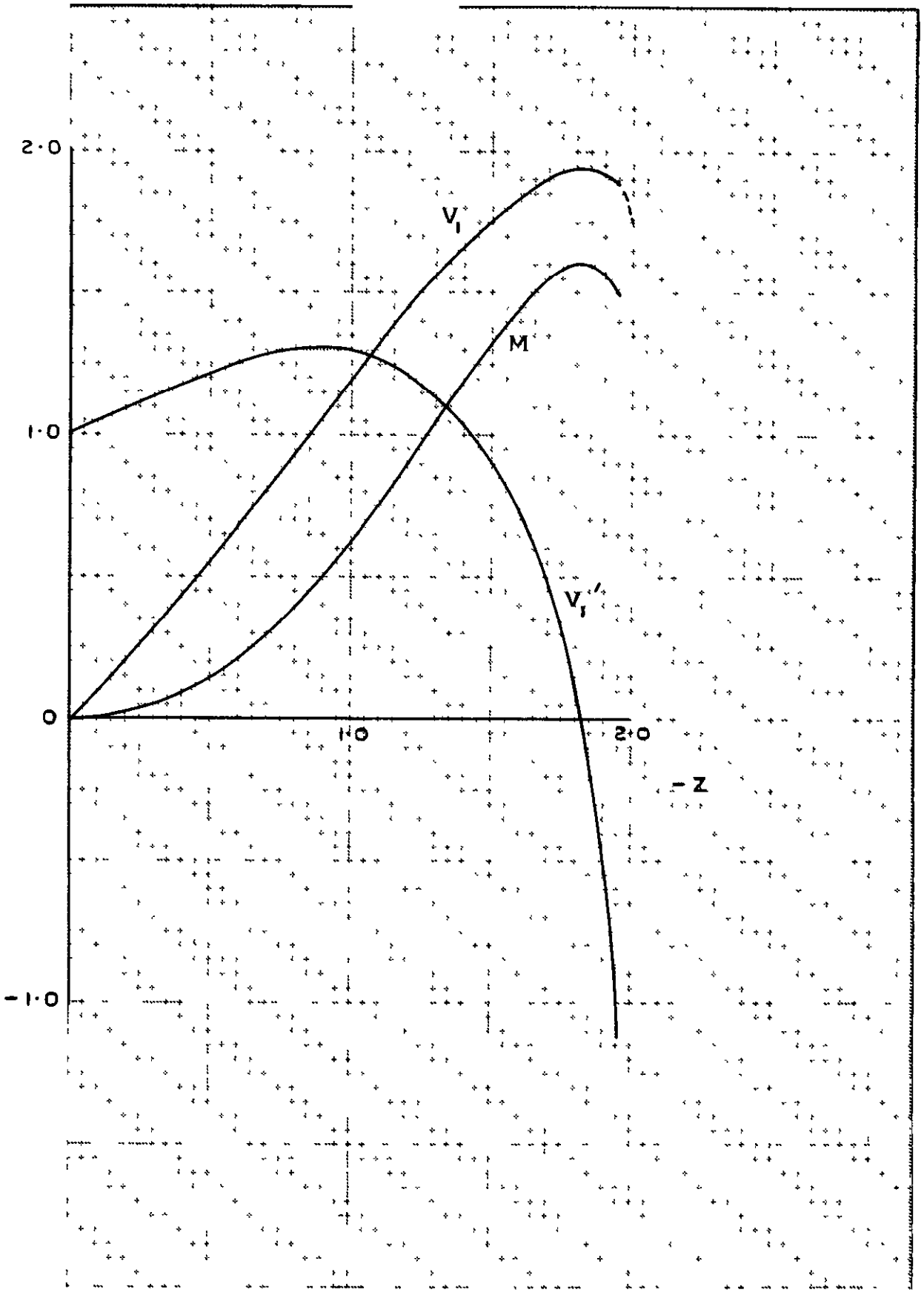

FIG.23 THE FUNCTIONS V_1', V_1, AND M (SEE APPENDIX)

Printed in England for Her Majesty's Stationery Office by the Royal Aircraft Establishment, Farnborough. Dd.125875. K5.

A.R.C. C.P. No.884 532.542.1 :
May 1965 533.697.2 :
533.6.011.5

Roe, P.L.

AN EXPERIMENTAL INVESTIGATION OF THE FLOW THROUGH INCLINED CIRCULAR TUBES AT A MACH NUMBER OF 4.0

Pressure plotting experiments have been performed on the internal flow through inclined circular tubes at M = 4, and the results used to investigate both the nature of the flow and the internal forces. It is intended to apply the results to the wind tunnel testing of models with nacelles. Linear theory calculations have been made and the predicted forces are in good agreement with experimental values, provided the ducts are short.

A.R.C. C.P. No.884 532.542.1 :
May 1965 533.697.2 :
533.6.011.5

Roe, P.L.

AN EXPERIMENTAL INVESTIGATION OF THE FLOW THROUGH INCLINED CIRCULAR TUBES AT A MACH NUMBER OF 4.0

Pressure plotting experiments have been performed on the internal flow through inclined circular tubes at M = 4, and the results used to investigate both the nature of the flow and the internal forces. It is intended to apply the results to the wind tunnel testing of models with nacelles. Linear theory calculations have been made and the predicted forces are in good agreement with experimental values, provided the ducts are short.

A.R.C. C.P. No.884 532.542.1 :
May 1965 533.697.2 :
533.6.011.5

Roe, P.L.

AN EXPERIMENTAL INVESTIGATION OF THE FLOW THROUGH INCLINED CIRCULAR TUBES AT A MACH NUMBER OF 4.0

Pressure plotting experiments have been performed on the internal flow through inclined circular tubes at M = 4, and the results used to investigate both the nature of the flow and the internal forces. It is intended to apply the results to the wind tunnel testing of models with nacelles. Linear theory calculations have been made and the predicted forces are in good agreement with experimental values, provided the ducts are short.

DETACHABLE ABSTRACT CARDS

Published by
HER MAJESTY'S STATIONERY OFFICE
To be purchased from
49 High Holborn, London W C 1
423 Oxford Street, London W 1
13A Castle Street, Edinburgh 2
109 St Mary Street, Cardiff
Brazennose Street, Manchester 2
50 Fairfax Street, Bristol 1
35 Smallbrook, Ringway, Birmingham 5
80 Chichester Street, Belfast 1
or through any bookseller

S.O. CODE No. 23-9016-84